




Energy-Efficient Emerging Optical Wireless Links

George K. Varotsos ¹, Konstantinos Aidinis ², Hector E. Nistazakis ¹ and Zoran Gajic ^{3,*}

¹ Section of Electronic Physics and Systems, Department of Physics, National and Kapodistrian University of Athens, 15784 Athens, Greece; georgevar@phys.uoa.gr (G.K.V.); enistaz@phys.uoa.gr (H.E.N.)

² Department of Electrical and Computer Engineering, Ajman University, Ajman P.O. Box 346, United Arab Emirates; k.aidinis@ajman.ac.ae

³ Electrical and Computer Engineering Department, Rutgers University, 94 Brett Road, Piscataway, NJ 08854-8058, USA

* Correspondence: zgajic@soe.rutgers.edu; Tel.: +1-(848)-445-3415

Abstract: In recent years, the tremendous increase in data traffic carried by wireless communication networks has generated the urgent need for establishing more energy-efficient wireless communication systems. Recent advances in semiconductor and light devices have triggered remarkable research interest to the development of these optical wireless communication (OWC) links. Among them, free-space optical (FSO) links and, more recently, ultraviolet links which operate within the (UV-C) spectral band, have been considered as prime candidates to create both high speed and power effective line-of-sight (LOS) and non-light-of-sight (NLOS) free-air communication links, respectively. Moreover, transdermal optical wireless (TOW) links for telemetry with medical implants minimize the expense of power for the implant. In the current review, a background on the energy efficiency challenges in wireless communication is presented. Each of these OWC technologies is mainly discussed in terms of key energy consumption requirements and major limiting factors that affect their power performance. Energy-efficient modulation formats as well as other powerful techniques for performance enhancement such as diversity and relaying are assessed. The survey is concluded with a discussion regarding their future energy consumption requirements and trends.

Keywords: energy-efficient communications; optical wireless communication links; ultraviolet links; free-space optical links; transdermal optical wireless links



Citation: Varotsos, G.K.; Aidinis, K.; Nistazakis, H.E.; Gajic, Z.

Energy-Efficient Emerging Optical Wireless Links. *Energies* **2023**, *16*, 6485. <https://doi.org/10.3390/en16186485>

Academic Editor: Andrea Mariscotti

Received: 30 July 2023

Revised: 2 September 2023

Accepted: 4 September 2023

Published: 8 September 2023



Copyright: © 2023 by the authors. Licensee MDPI, Basel, Switzerland. This article is an open access article distributed under the terms and conditions of the Creative Commons Attribution (CC BY) license (<https://creativecommons.org/licenses/by/4.0/>).

1. Introduction

In recent years, the wireless communication bandwidth traffic has witnessed a dramatically rapid increase which has rendered the traditional radio frequency (RF) spectrum almost overcrowded [1–3]. It is worth mentioning that the International Data Corporation's recent report expects 22 billion active Internet of Things (IoT) devices in 2018 to attain 41.6 billion in 2025, producing 79.4 zettabytes of data. Additionally, Cisco's 2018–2023 Annual Internet Report claims that more than two-thirds of total traffic is caused by mobile wireless devices. It is expected that from 2027 to 2030, the sixth generation (6G) wireless communication systems, fully supported by artificial intelligence, will become an effective approach to wireless communication [1,4]. Considering this exponentially growing need for more smart wireless devices that accommodate higher capacities with higher security level operating at the lowest possible power consumption, remarkable research and industrial attention has been lately attracted to the transition to the optical spectrum, as demonstrated by the continual emergence of even newer high-capacity services and varying sophisticated applications. OWC systems that operate within this bandwidth-effective and energy-efficient optical spectral range have made tremendous strides in the last few years in both telecommunication and biomedical fields [2,5].

In basic terms, OWC technology utilizes a light information-bearing carrier, i.e., an infrared, a visible or an ultraviolet light wave, which is propagated in both indoor and

outdoor environments through unguided channels including atmosphere, underwater, space or even skin, in an attempt to convey the information signal from one point to another [6]. In the case of employing infrared light waves, we usually refer to infrared (IR) or free-space optical (FSO) communication systems, with indoor IR operating mainly within 780–950 nm and outdoor FSO systems operating mainly at 1550 nm [7]. When employing visible light waves, we usually refer to indoor visible light communication (VLC) systems operating within 380–780 nm [8]. In the same context, when utilizing ultraviolet (UV) light carrier, and specifically from the C band of ultraviolet light spectrum (100–280 nm) which is commonly used for communication applications, we refer to indoor or outdoor UV-C communication systems [9]. In the specific case that the transmission medium is skin, while the operational light wave is chosen within the so-called medical optical window (600–1300 nm), we refer to transcutaneous or transdermal optical wireless (TOW) communication systems [10–12].

What all of the above OWC modalities have in common is that by increasing the information-bearing carrier frequency to that of light waves, it becomes viable to increase the achievable data rates by many orders of magnitude in comparison with their millimeter wave (MMW), terahertz (THz), and much less, with their conventional RF counterparts [2,13]. It is notable that the latter happens by consuming less power in comparison with the mentioned other technologies, which is a vital requirement toward the worldwide goal to reduce energy consumption. In addition, outdoor free-air OWC are generally more challenging than indoor ones mainly due to the random nature of atmospheric channel, while between IR FSO and UV-C, the former outperforms in terms of coverage area but only for LOS stationary transceiver terminals, whereas the latter supports shorter NLOS links where transceivers' mobility is potentially enabled. In regards to indoor OWC, perhaps the most challenging direction is the recently emerging TOW technology mainly due to the complexity of skin in comparison with free-air indoor channels.

In the current literature review, we focus on outdoor terrestrial FSO, outdoor UV-C, and TOW communication systems. Taking also into consideration that the vast majority of relative reviews reported to date are on the open OWC technical literature, we are mainly focused on wireless channel modeling as well as on the capacity, coverage area, and outage performance of these OWC links [4,6–10,14–19]. In this literature review, we incorporate and highlight the energy efficiency of these OWC systems by means of their power consumption. The paper is structured as follows. Terrestrial outdoor FSO based on IR that henceforth will be briefly referred to as FSO and presented in Section 2. In Section 3, UV-C is outlined, and TOW is covered in Section 4, followed by the discussion and the conclusions section.

2. Terrestrial FSO

Terrestrial FSO communication is in basic terms a LOS technology transferring information from one point to another, via light waves through atmospheric channels operating at wavelength regions of 850 nm, 1300 nm, and 1550 nm corresponding to the first, second, and third optical fiber, respectively [20–23]. Therefore, by using appropriate laser sources and photo-detector apertures at transmitter and receiver terminals, respectively, FSO can be utilized in a variety of applications including establishment of high-capacity links between buildings, buildings to optical fiber networks, as well as between points located in difficult terrains where fiber infrastructure is not feasible or it is very expensive, such as across rivers or very busy streets. Additionally, FSO can be used as a prime solution for the last-mile access network, the wireless cellular communication back-haul, as well as for disaster recovery by creating temporary and/or complementary optical links. Moreover, FSO links are immune to electromagnetic interference (EMI) and multi-path dispersion, and they guarantee high-security levels due to the narrow information-bearing light propagating beams, which make any undesirable interference difficult. They operate with low power consumption and cost within the unregulated FSO spectrum, while they are significantly flexible for deployment and redeployment due to their compact equipment and easy installation [2,8,24,25].

The deployment of FSO is hindered by different performance limiting factors that mainly originate from the random nature of the atmospheric channel. In fact, effects of fog, rain, snow, hail, solar radiation along with atmospheric gases, aerosols, molecules, atoms, and air-borne particles lead to beam attenuation due to photon absorption and scattering that results, in turn, in extinguishing and changing the direction of photons. Specifically, similarly to our view of distant object, the FSO transmission is significantly hampered by fog. This is due to the fact that infrared optical wavelengths and fog droplets have a comparable size, generating much scattering of the laser energy as fog is getting thicker [26–29]. Under thick and dense fog channel conditions, attenuation due to photon scattering can exceed 30 dB/km, which may limit the practical FSO coverage area over a range of up to 500 m, whereas FSO performance is not strongly degraded by rain (only about 3 dB/km) [27]. A first idea to overcome photon scattering under the presence of thick and dense fog, could be to sufficiently increase the power to be transmitted. Nevertheless, this not only leads to energy-inefficient communication links, but also it may exceed the eye-safety limits. Although attenuation due to photon scattering is not a wavelength-dependent effect, the allowable safety for the eye laser power should be fixed at 1550 nm. In fact, it is about 50 times higher at 1550 nm in comparison with 850 nm, offering up to 17 dB additional power margin [30]. Consequently, for a given propagation distance, operating at 1550 nm instead of operating at 850 nm results in significantly more energy-efficient FSO links, as it is representatively illustrated in Table 6 of [30]. On the other hand, contrary to attenuation due to scattering, attenuation due to absorption is wavelength dependent, and hence selective. Once again, the region of 1550 nm should be selected. Among the appropriate optical transmission windows mentioned above, this wavelength region provides the minimum photon absorption by constituents of the atmospheric channel, alike. The latter also applies to optical fiber systems, making the FSO and optical fiber connectivity a flexible process without resorting to the use of any wavelength converters. It should be noted here that in exceptionally clear weather, the attenuation due to photon scattering through the atmosphere is almost 0.2 dB/km (at 1550 nm) [31], and thus equal to the attenuation in a typical optical fiber, which enables the propagating laser beam not to waste any significant amount of energy by propagating from free air to the fiber, and vice versa. In short, by selecting 1550 nm as a FSO information-bearing carrier, we can significantly mitigate the negative side effects of channel-induced signal's attenuation, especially in an exceptionally clear sky, creating energy effective, environmental friendly, and safety for health optical wireless transmissions.

A major unavoidable impairment of energy efficiency and the performance of FSO links is the atmospheric turbulence stochastic effect, which stems from changes in the refractive index of the atmospheric propagation path, owing to in-homogeneities in temperature and rapid pressure variations in the atmospheric channel [2]. Even in a very clear sky, and primarily over propagation distances of the order of 1 km or longer, atmospheric turbulence generates the so-called scintillation effect, which brings about random variations of the irradiance of signals arriving at the receiver side [32,33]. In more detail, the atmospheric turbulence effect originates from solar radiation absorption by the earth's surface, which makes the air around it warmer in comparison with the air at higher altitude. Being less dense, the warmer air rises to mix turbulently with the layer of the surrounding cooler air, which leads the atmospheric temperature to randomly change. These temperature fluctuations that are heavily related to atmospheric pressure, altitude, and wind speed result in atmospheric refractive index variations. These in-homogeneities can be emulated through distinct eddies of different temperatures operating as prisms of varying sizes and refractive indices. Consequently, the interaction between the propagating light beam and the turbulent atmospheric medium leads to random phase and intensity fluctuations of the received signal, which are commonly reported as turbulence-induced scintillation effect [2,22]. The known effect of turbulence-induced scintillations is the twinkling of the stars due to their random irradiance variations and the shimmering of the horizon on a hot day generated by random fluctuations in the light beam's optical phase, which

results in reduced image resolution [34]. According to turbulence strength, FSO signal scintillations can be emulated through varying statistical distribution models, as reported in [32,35–42]. Among them, for weak to moderate turbulent channels, it is common practice to use lognormal (LN) [32] or for simplicity reasons the Gamma distribution model [36]. For strong to very strong turbulence, we should use the suitable K-distribution [40], whereas for extremely strong to saturated turbulence, the negative exponential distribution model is appropriate [41]. Alternatively, over a wide turbulence regime, i.e., for weak to very strong turbulence conditions, it is wise to move to unifying models by using either the most commonly reported Gamma–Gamma (G–G) distribution or the more recent Malaga distribution that were introduced in [35] and [37], respectively. In brief, atmospheric turbulence is a very complex and stochastic effect that hampers optical beam’s propagation through the atmospheric channel, especially for longer propagation distances, causing beam wander, beam spreading, as well as beam scintillation, which result in undesirable fluctuations in the spatial power density at the receiver plane, degrading the energy efficiency and reliability of FSO systems.

In addition to the above mentioned, another significant concern in FSO development is the pointing errors effect, i.e., unavoidable and stochastic beam misalignments that alter the LOS requirement between transmitter and receiver apertures. Effects of thermal expansion, strong wind, and weak earthquakes cause the sway of high buildings, where FSO transceivers are mostly located [43]. The latter brings about optical beam vibrations that result, in turn, in misalignment-induced intensity fluctuations of the optical signal arriving at the photo-detector aperture. This misalignment-induced fading is commonly known as the pointing errors effect. Owing to the stochastic nature of pointing errors, statistical distribution models are utilized to emulate misalignment-induced signal fluctuations. The most widely utilized pointing errors model was proposed in [44]. It is a Rayleigh distribution-based model, which takes into consideration the beam width, pointing error variance, and detector aperture size [45]. Through this model, the boresight component of pointing errors has been assumed to be equal to zero. To be precise, pointing errors contain two components, i.e., boresight and jitter. The boresight denotes the fixed displacement between the beam and the photo-detector aperture center, whereas jitter represents the random offset of the beam at detector plane. In this respect, a more generalized pointing errors model is needed to include boresight effects. Indeed, the authors of [46] presented this more composite pointing errors approach with boresight via the versatile statistical analysis. More recently, the authors of [47] introduced an accurate simplified approximation of Beckman distribution model, which can be used to model non-zero boresight pointing errors with a high level of accuracy. Here, it is noted that the joint influence of turbulence-induced and misalignment-induced fading can be estimated through the combined probability density function of their distribution models mentioned above, as considered in [44–50].

In view of the above, even in a clear sky where attenuation due to atmosphere is not the prime limitation, the joint impact of turbulence-induced and misalignment-induced fading reduces the level of the collected optical power at the receiver’s input. In order to overcome this energy loss issue, in many cases, it is required to increase the transmitted power (provided that it is feasible), which increases the energy consumption, and therefore degrades the energy efficiency of the FSO system. It is wise thus to move in the direction of employing more energy-efficient FSO methods, techniques, and configurations.

To this end, useable modulation techniques are able to play a key role. Among them, it is well known that on-off keying (OOK) is significantly the most widely employed modulation scheme mainly due to its simplicity and compactness. Nevertheless, when it is utilized under fading conditions, the detector threshold should be evaluated and adopted by appropriate means, in agreement with different states of the propagation medium. This disadvantage can be circumvented via L -symbol pulse position modulation (L -PPM) technique, which outperforms OOK by means of power efficiency, given that L is at least equal to four [2,51–53]. The latter takes place at the expense of higher complexity and

lower spectral efficiency that is of minor impact, bearing in mind the enormous available unregulated optical bandwidth along with the urgent trend to save energy. Alternatively, we can resort to more complex and sophisticated modulation formats such as subcarrier intensity modulation (SIM) with the phase shift keying (PSK) or quadrature amplitude modulation (QAM) and orthogonal frequency division multiplexing (OFDM) modulation techniques. Although these SIM modulation formats can improve significantly the performance metrics, they experience two critical issues. The first one is that supporting multiple subcarriers leads to a higher power consumption requirement. The second problem is that by employing PSK or generally a phase coherent approach, this requires a precise carrier phase synchronization between emitted and received signals. Nevertheless, perfect phase evaluation of the received signal is unfeasible in reality, mainly owing to practical hardware imperfections at the PSK demodulator, which generates phase noise effects that are usually well described by the well-known Tikhonov distribution [54,55]. In view of the above, the power efficiency and the dominant criterion for the operation of a FSO link, *L*-PPM should be selected.

In addition, it has been demonstrated in [2,56–63], among numerous other papers in the open technical literature, that the diversity method is a very effective technique to address the major limiting factors that degrade the FSO performance and availability. In fact, when the propagation distance is within the required limits, but the FSO system's availability underperforms, the diversity technique is a good solution to enhance it in an adequate energy-efficient manner. In basic terms, diversity stands for the consideration of multiple copies of the propagated signals in an intention to effectively address a poor transmission channel state and enhance the total reliability and performance of the communication system [58]. In general, diversity can be implemented in space, in time, or in wavelength [56]. Employing diversity in space, which is commonly known as spatial diversity [56,57], a FSO system incorporates multiple transmitters and/or receivers at different places but in very short distances that transmit and receive copies from the same signal, leading to a lower error probability. In the case of time diversity schemes [59,63], the system utilizes a single transmitter-receiver pair, so that the signal is retransmitted at different time slots. Finally, when wavelength diversity is employed [58,61], FSO sources use a composite transmitter so that the information signal is transmitted at the same time but at slightly different wavelengths toward the corresponding proper receivers. Consequently, via diversity, a single input-single output (SISO) FSO link can be upgraded into a more effective performance, in terms of the error rate and reliability of either single input-multiple output (SIMO), multiple input-single output (MISO) or multiple input-multiple output (MIMO) FSO system. Instead of increasing the transmitted power to achieve improved availability results, we may utilize a spatial diversity system configuration that incorporates SIMO links without increasing the power level of the emitted optical signal. In these cases, the diversity method can achieve very energy-efficient availability enhancements.

Furthermore, when the coverage area of the FSO link needs to be extended, the serial relaying technique is significantly the most suitable, in which case the optical signal is emitted from the transmitter and arrives at the receiver via intermediate serially connected nodes. These intermediate nodes may be either amplifiers or decoders. In the former case, the intermediate nodes are commonly known as amplify and forward (AF) relays since the received intermediate signal is simply amplified and then forwarded to the next node. Nevertheless, considering the presence of noise which is also amplified, the beneficial propagation distance cannot be significantly extended. In the latter case, the intermediate nodes are commonly known as decode and forward (DF) relays since they decode the intermediate received signal to forward it to the next node, while having the advantage of getting rid of the noise in the signal, they can achieve longer total propagation distances in comparison to their AF counterparts. Specifically, in serial DF relaying configurations, alternatively known as multi-hop DF relaying configurations, the source transmits the information signal to its nearest DF relay node that decodes the detected signal, modulates it, and retransmits it to the next DF relay or destination node only if the received signal to

noise ratio (SNR) exceeds an appropriate decoding threshold that guarantees the proper and reliable operation of the FSO system. The latter procedure continues until the information-bearing signal arrives at the input of the destination node [25,64]. In regard to the critical goal of energy efficiency through multi-hop DF relaying, we can adequately extend the initial FSO link length without consuming extra transmitted power, as we should perform in the case of not using any intermediate DF relay across the link. On the contrary, in parallel DF relaying that is also known as cooperative diversity, the laser source transmits the same signal at the same time to all relay nodes, which, in turn, decodes and retransmits the signal to the destination, provided that the SNR values at the DF relay inputs are larger than the corresponding threshold values. It should be also mentioned that parallel relaying has been shown to be more efficient when the reliability and availability of the FSO link need to be enhanced without consuming a larger amount of transmitted power [24]. Therefore, by properly combining serial and parallel relaying configurations, mixed relaying architectures can be created [24,33] which both extend the initial link length and, at the same time, improve the total FSO availability to a satisfactory level, without energy cost by means of further increasing the power to transmit.

Another effect that may affect the FSO propagation, which has not yet been thoroughly investigated for practical FSO links in the open technical literature, is the group velocity dispersion (GVD) effect. This effect is generated by the fact that the transmitted information-bearing laser signal is not entirely monochromatic but comprises different spectral components that are not traveling with the same velocity through the dispersive atmospheric path. It has been proven in [49,65–67] that GVD results in temporal shape alterations of the propagating FSO pulses. Specifically, for non-negative chirped initial pulses, GVD results in temporal broadening, which may result in a problematic signal's identification at the receiver's side along with the interference between consecutive pulses. Conversely, it has been shown in [49,65–67], that by adjusting the initial pulses to be negative chirped, i.e., for chirp parameter $C < 0$, GVD results in temporal narrowing, which can enhance the erroneous performance, and thus extend useable link distance. It is notable that the latter beneficial impact of GVD does not require a larger amount of optical power and, in this respect, it is energy efficient. In any case, GVD's influence is getting stronger for shorter and chirped initial pulses, which are propagating across longer propagation distances. In this respect, GVD should be taken into account for the design of modern energy-efficient FSO links that cover larger propagation distances with shorter pulses, and therefore with higher achievable data rates.

To date, the investigation of real FSO systems in the open technical literature demonstrates several impressive energy-efficient performance results. Unless otherwise stated, the FSO links described in the representative publications below operate under clear weather conditions, weak turbulence, and pointing errors, as well as with OOK modulation formats. Authors in [68] established an aerostat to ground FSO link that operated in the 1530–1560 nm wavelength region. For a FSO link, the distance of 1.4 km achieved a capacity of 80 Gbps with a BER at 10^{-6} , consuming an optical transmit power from 20 to 26 dBm, i.e., an average transmit power equal to 199.53 mW. The authors in [69], in Pisa, Italy, established between two buildings a roof-to-roof FSO link of a distance of 212 m to perform several experimental tests. Operating at 1548.51 nm, they achieved 40 Gbps with BER = 10^{-9} with the required power being almost equal to -27.5 dBm, i.e., 1.778 μ W. Note that under these circumstances, by using the wavelength division multiplexing (WDM) technique, they upgraded this system to achieve 1.28 Tbps (32×40 Gbps). The authors in [70] in Graz, Austria, established three different FSO links of 80 m, 650 m, and 2700 m, respectively with the operation wavelength being fixed at 950 nm. Transmitting the same amount of power equal to 6.0206 dBm, i.e., 4 mW, they achieved a capacity of 2.5 Gbps within the acceptable BER limits. Note that data rates could exceed 2.5 Gbps without increasing the transmitted power, especially for the shorter link configuration. However, the latter could not be realized, owing to the practical limitations of optic and electronic available equipments. The authors of [71] established a FSO link of 11.5 m operating at

1550 nm. By transmitting an optical signal with 10 dBm power, i.e., 10 mW, they achieved a data rate of 320 Gbps at $\text{BER} = 10^{-3}$ through 16-QAM modulation format with 40 Gbaud symbol rate. Note also that the power loss was 0.5 dB over 11.5 m link length, which indicates the feasibility to extend the link distance up to hundreds of meters, since we have catered for the strict alignment between transmitter and receiver apertures in order not to trigger strong pointing errors. Additionally, it is notable that by supporting 12 subcarriers covering 300 GHz with 25 GHz spacing through 16-QAM modulation, a maximum baud rate of 23 Gbaud has been achieved, which corresponds to 2.208 Tbps data rate at $\text{BER} = 10^{-3}$. Furthermore, authors in [26], outlined that for a transmitted power of 22 dBm, i.e., 158.49 mW, that is available nowadays in the FSO market, we can achieve $\text{BER} = 10^{-7}$ for a link length of 500 m under light fog conditions, whereas as fog is getting thicker, i.e., for more adverse fog types, BER becomes larger than 10^{-3} . In the same context, the achievable ergodic capacity for the latter link was equal to 30 b/s/Hz, 18 b/s/Hz or 5 b/s/Hz for light, moderate, and dense fog, respectively. It is recalled that the ergodic capacity, which is also known as average capacity, represents the expectation of the instantaneous channel capacity (maximum data rate that the channel can accommodate), and it has significance when the channel variations are very fast in comparison to the symbol duration. It can be estimated by means of the expectation of the mutual information expression with respect to random fading coefficients (such as turbulence-induced and misalignment-induced fading). Moreover, it has been shown that by decreasing the link length to 200 m in order not to emit more than 22 dBm, the achievable BER was smaller than 10^{-10} and approximately equal to 10^{-3} under moderate and thick fog conditions, respectively. The latter indicates the potential of establishing reliable and energy-efficient FSO links of 200 m in length, from light to even thick foggy channels.

The authors of [72] investigated a coastal FSO link of 70 m in length, established near the Red Sea (Thuwal, Saudi Arabia). The link could operate with a matched wavelength pair at 1330 nm/1550 nm. Even in the particularities of coastal environment, including adverse humidity and temperature variations, by consuming transmitted power of 0 dBm, i.e., 1 mW, the FSO link supported data rates of 1 Gbps, under acceptable BER limits. More recently, authors in [73] evaluated the performance of a FSO link established at an altitude of 35 m over sea surface through a coastal maritime channel between the building of Hellenic Naval Academy and the lighthouse of Psitalia Island, in Greece. The link had a total length of 2958 m, most of which is over sea, as well as it utilized a commercial MRV TS500/155 transceiver, operating with a maximum output power of 150 mW at 0.85 μm offering a data rate of 155 Mbps. It could also utilize up to three lasers with a beam divergence of 2 mrad each and a receiver with a radius of 10 cm, sensitivity of -46 dBm, and a photodetector of avalanche photodiode (APD). Additionally, in this maritime environment, NAVSLaM model has been proposed and utilized to estimate the refractive index structure parameter values, which are proportional to atmospheric turbulence strength. Under these circumstances, it has been shown that the link can adequately operate with reasonable energy efficiency in this challenging environment from weak to even strong turbulence conditions.

Regarding the use of L -PPM formats with a goal to achieve more power efficient practical FSO links, more practical work needs to be carried out. In this context, in [52], the use of 256-PPM without coding demonstrated an amelioration of about 5 dB at a fixed bit error rate (BER) of 10^{-6} in comparison to OOK. Theoretically, increasing L would continuously upgrade the power efficiency, but technical factors like synchronization and detection restrict this increase up to a reasonable value. The authors of [53] assessed the use of PPM in terms of the average symbol error probability (ASEP) metric. Their findings revealed that under weak turbulence conditions, by using 16-PPM format, there is a need for signal to noise ratio (SNR) of 32 dB to achieve ASEP of 10^{-3} , whereas under the same circumstances, by using OOK, there is a need for SNR at 38 dB to achieve the same ASEP of 10^{-3} . Recently, the authors in [2] adopted in their average bit error rate (ABER) analysis, several experimental data measurements carried out in University of Waseda, Japan, for

a real FSO link located there which was operating at 785 nm, with the receiver aperture having a diameter of 10 cm. The link length was equal to 1 km while it was established at a typical altitude of 25 m. Note that the optical power transmitted was 11.5 dBm, i.e., 14.125 mW. Under weak to strong NZB pointing errors and turbulence, the link could utilize apart from OOK, 4-PPM and 8-PPM, as well as the diversity method by using one transmitter and multiple (two or three) receivers, i.e., SIMO links. Increasing both diversity and modulation order significant ABER performance enhancements have been presented, especially for weak turbulence and generalized pointing errors. For example, to achieve an average BER equal to 10^{-5} , the employment of 4-PPM configuration is shown to require almost 5 dB less versus the corresponding (2-PPM or OOK) configuration. Note that this performance and availability improvements are realized by consuming an acceptable amount of power, as well as the fact that reasonable ABER results have been obtained in comparison with corresponding findings in [48], which investigated the SISO configuration of the same practical link with the same transmitted power of 11.5 dBm, i.e., 14.125 mW. The potential of employing multi-hop DF relay configurations for this link has been investigated in [64], for different SIM PSK modulation formats. It has been shown that for less complex PSK constellations of lower order, it is feasible to significantly extend the link in a power-efficient mode, especially under weak turbulence, generalized pointing errors, and phase noise effects. Indeed, it has been illustrated that doubling the link length by means of a dual-hop DF relay configuration, an average SNR of 30 dB was needed to achieve a total ASEP equal to 2.9×10^{-3} through SIM 4-PSK format, for weak turbulence along with a weak amount of pointing mismatch and moderate phase noise effects.

Table 1 below summarizes and presents some key parameter values that illustrate the energy efficiency and the total achievable performance for some significant practical FSO systems and link configurations mentioned above. In this context, Table 1 provides a quick overview and comparison among the impact of each effect and technique described above. Furthermore, in Figure 1, the possibilities and energy-efficient applications of FSO communication systems along with the limiting factors on their performance and energy consumption, are presented.

Table 1. Major practical FSO systems and representative link configurations.

Ref.	Turbulence Model	Pointing ERRORS	Modulation Technique	FSO System Configuration	Diversity Method	Transmitted Power	Data Rate	Link Length	BER	ASEP/Pf
[68]	-	-	OOK	SISO	-	199.53 mW	80 Mbps	1.4 km	10^{-6}	-
[69]	-	-	OOK	SISO	-	1.778 μ W	40 Gbps	212 m	10^{-9}	-
	-	-	OOK	WDM	-	1.778 μ W	1.28 Tbps	212 m	10^{-9}	-
[70]	-	-	OOK	SISO	-	4 mW	2.5 Gbps	2.7 km	$<10^{-9}$	-
[71]	-	-	16-QAM	SISO	-	10 mW	320 Gbps	11.5 m	10^{-3}	-
	-	-	16-QAM	WDM	-	10 mW	2.2 Tbps	11.5 m	10^{-6}	-
[26]	-	-	OOK	SISO (clear)	-	158.49 mW	30 b/s/Hz	500 m	10^{-7}	-
	-	-	OOK	SISO (fog)	-	158.49 mW	18 b/s/Hz	500 m	10^{-3}	-
[72]	-	-	OOK	SISO (coast)	-	1 mW	1 Gbps	70 m	-	-
[73]	NAVSLaM	-	OOK	SISO (coast)	-	150 mW	155 Mbps	2958 m	-	-
[2]	Malaga (strong)	ZB (weak) NZB (weak)	4-PPM 4-PPM	SISO SIMO	- Spatial	14.125 mW 14.125 mW	- -	1 km 1 km	2.2×10^{-3} 3×10^{-5}	- -
[2]	Malaga (weak)	ZB (weak) NZB (weak)	4-PPM 4-PPM	SISO SIMO	- Spatial	14.125 mW 14.125 mW	- -	1 km 1 km	1.8×10^{-4} 7×10^{-7}	- -
[2]	Malaga (moderate)	NZB (strong) NZB (strong)	OOK 8-PPM	SIMO SIMO	Spatial Spatial	14.125 mW 14.125 mW	- -	1 km 1 km	10^{-3} 10^{-4}	- -
[2]	Malaga (moderate)	NZB (weak) NZB (weak)	OOK 8-PPM	SIMO SIMO	Spatial Spatial	14.125 mW 14.125 mW	- -	1 km 1 km	4×10^{-5} 2×10^{-7}	- -
[64]	Malaga (weak)	NZB (weak) NZB (weak)	4-PSK 4-PSK	Single-hop Dual-hop	- -	14.125 mW 28.25 mW	- -	1 km 2 km	- -	1.5×10^{-3} 2.9×10^{-3}
[65]	G-G (weak)	-	OOK OOK	SISO ($C > 0$) SISO ($C < 0$)	- -	20 mW 20 mW	- -	10 km 10 km	- -	3×10^{-3} 2×10^{-3}

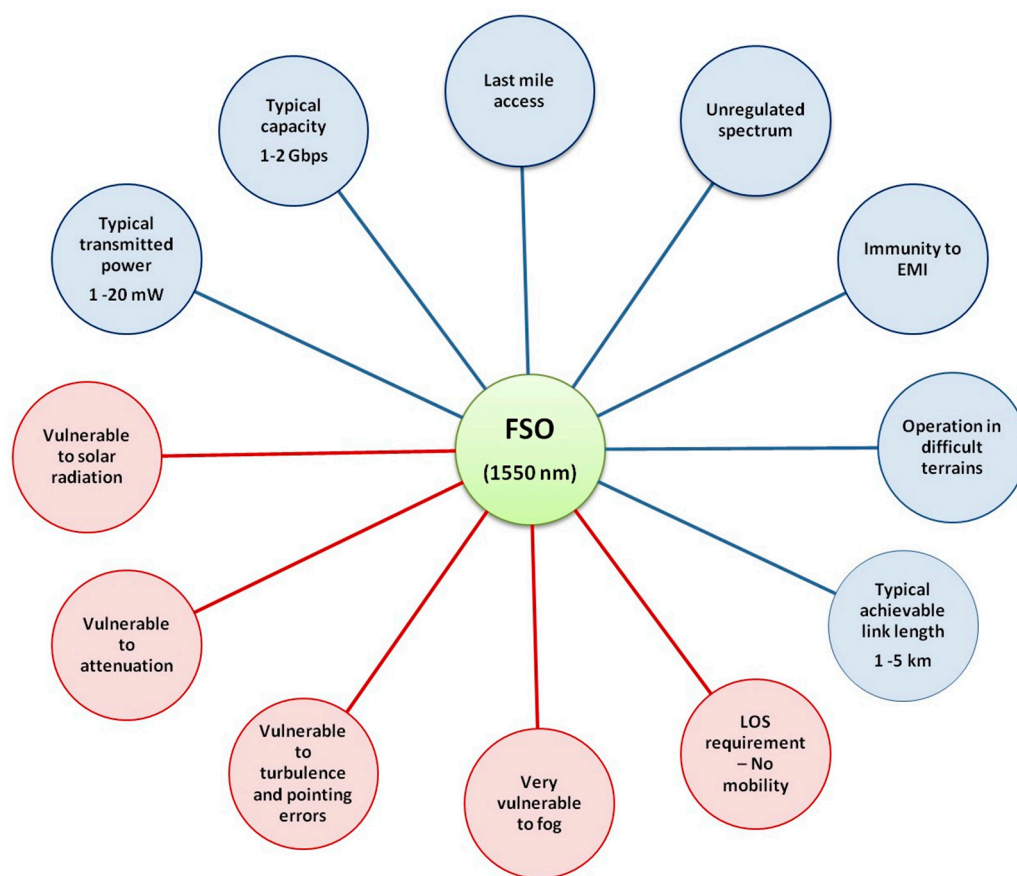


Figure 1. Possibilities and energy-efficient applications of FSO communication systems, illustrated with blue color, versus adverse issues and limiting factors on their performance and energy consumption, illustrated with red color.

3. Ultraviolet Communication

The remarkable evolution of UV devices including UV light-emitting diodes (LEDs), UV laser semiconductors, solar-blind UV optical filters, and sophisticated UV light detectors, such as photomultiplier tubes (PMTs) and UV avalanche photo diodes (APDs), have enabled the exploitation of the very promising deep UV band (UV-C) for high-bandwidth and energy-efficient wireless communications [9,16,74–76]. In fact, UV band is in a wavelength range within 100–280 nm, which is solar blind at the sea level causing the solar noise to be negligible in this range due to strong absorption by the ozone layer in the upper atmosphere. Additionally, contrary to FSO that operates in the infrared band, the UV-C band provides the novel opportunity of establishing NLOS optical communication links with low-power consumption. This enhances the potential of mobility, and it is very crucial when FSO LOS path is not feasible to be installed or might be either blocked or impeded by obstacles. The large and unregulated spectrum in the UV band has the potential to support high rate services, a few times higher than its FSO counterpart [75]. Another significant point in favor of UV-C links compared with their FSO counterparts is their robustness against adverse weather conditions and strong scattering that enables the NLOS feasibility [9]. Since the scattered intensity has been proven to be inversely proportional to the fourth power of the wavelength, the shorter wavelength is significantly scattered, especially for UV carrier [8]. Nevertheless, the UV deployment suffers mainly from atmospheric turbulence and atmospheric channel attenuation. In addition, cloud depth, rain, and fog may have a negative influence on UV signal transmissions [42]. Note that UV-C links are affected to a greater extent than FSO by atmospheric turbulence and scattering, whereas to a lesser extent by pointing errors due to their NLOS potential.

MIT Lincoln Lab first created a LED-based testbed, reported with a NLOS medium [77]. The researchers employed 10 LED units at 274 nm, with each LED unit having a 24-element array, for 240 LEDs emitting a total optical power of 40 mW. At the receiver, a proper PMT was combined with an appropriate solar blind optical filter to provide a high solar noise rejection ratio. The system achieved a data rate of 2.4 kb/s employing 4-array pulse position modulation (PPM) at a distance of 11 m. Experimental measurements highlight range BER trade-offs and effects of several major system parameters, such as elevation and azimuthal angles between transmitter and receiver apertures, and the influence of optical filters and PMTs [78]. Research on semiconductor detectors for utilization in the deep UV-C band was also performed [79]. Considerable effort has been made in accurately describing the UV NLOS communication channel, which is heavily based on the complex interaction of the propagating UV signal with the atmosphere. These channel models basically estimate the path loss and/or the impulse response function of a UV link according to the corresponding link geometry, which incorporates the distance from transmitter to receiver along with key characteristics of the emitted UV beam and receiver field of view (FOV) [80]. The channel path loss determines the power level of the received UV signal, and thus the error performance for any implemented data modulation format. Therefore, the channel's path loss estimation is critical for assessing the necessary power consumption, and thus the energy efficiency for a reliable UV link's operation. On the other hand, the channel impulse response determines the pulse broadening effect due to scattering, providing signaling reference to avoid inter-symbol interference (ISI) [8]. In short, for the UV link ranges (typically below 200 m), the single scattering model fits well along with experimental measurements, whereas for the middle and long range UV communication, the multiple scattering model that relied on the Monte Carlo method is mostly utilized. Moreover, atmospheric turbulent effects should be incorporated. In this respect, several empirical path loss formulas that relied on a large amount of experimental results up to 100 m have been initially proposed [81–85]. For the longer regime UV links, the detrimental impact from fully coupled scattering and atmospheric turbulence that becomes more important have been initially investigated in [86–101]. In [86], preparatory models over a wide turbulence strength regime were proposed, highlighting that under certain geometric conditions, the collected scattered signals at the receiver input are averaged leading to a smoothed signal at the receiver output. A collection of data measurements of irradiance scintillations, expressed through the normalized variance, has been reported in [92]. It was shown that experimental measurements for a UV link length of 185 m matched well with their corresponding predicted values that relied on aperture averaging. In [93], the NLOS scintillation probability density function (PDF) was emulated by adjusting an existing LOS scintillation lognormal distribution considering two different LOS links. In order to achieve less cumbersome computation processes, the authors in [96] proposed a conjunction of both numerical and analytical methods. Experimental results regarding the effect of turbulence on the received signal energy distribution instead of the average path loss were collected in [97]. The researchers in [98] extended the latter by proposing a Monte Carlo channel model that takes into account the multiple scattering effects in turbulent channel's behavior. Under weak turbulent UV channels, a modified quality indicator that is well-known as scintillation attenuation, was estimated in [99]. Following this approach, the atmospheric extinction coefficient was properly adjusted and a novel analytical expression for the single scattering path loss model was derived. Recently, the key difference for turbulence-induced scintillations between UV-C and FSO channels, stemming from the large path loss of UV-C links, was assessed in [100]. It was revealed that the very weak signal received introduces a doubly stochastic process arising from the variations of the transmitted signal according to the lognormal distribution, while the number of detected photoelectrons follows the Poisson distribution. Note that authors in [93] had already proposed the lognormal distribution to emulate weak turbulence conditions in UV-C links. In this context, the authors in [102] assessed the energy efficiency of a 50 m point-to-point UV link by means of the achievable BER over a wide regime of power transmission values through a lognormal modeled weak

turbulent medium, by utilizing also different modulation formats, including OOK, PPM, as well as OFDM along with PSK. Being PPM the most energy-efficient modulation scheme as mentioned in the previous section, their findings highlighted that PPM outperformed in terms of low power consumption, as it was expected. Conversely, the less energy-efficient format was the non-return-to-zero (NRZ) OOK one. Specifically, by employing 4-PPM format, the required transmitted power was almost equal to 11 dBm, i.e., 12.59 mW to achieve $\text{BER} = 10^{-5}$, whereas through NRZ, the transmitted power was almost 13.3 dBm, i.e., 21.38 mW to achieve $\text{BER} = 10^{-5}$, as well. Bearing in mind that the LN model is one of the most accurate models for weak to moderate turbulence-induced scintillation in the traditional infrared FSO area, the latter findings paved the way to adopt, adjust, and incorporate several well-known FSO distribution turbulence models in the emerging UV-C area. Indeed, the unifying Malaga distribution has been recently introduced in [103] for weak to strong turbulent UV-C links, the generalized Gamma–Gamma distribution has been utilized in [104,105] under the same wide turbulent range and, more recently, the K-distribution has been employed in [106] for strong to very strong turbulent UV-C links.

It is remarkable that in [104–120], diversity techniques have been investigated and utilized either theoretically or experimentally, in order to enhance the total UV-C system's performance and availability toward an energy-efficient direction. Indeed, these illustrative successful examples are in [112], where for a target BER of 10^{-6} over a 1 km UV system operating at 260 nm, a SNR of 36 dB was required for the SISO configuration, while this requirement reduced to 33.5 dB and 32.5 dB, offering performance gains of 2.5 dB and 3.5 dB for MISO link configurations with two and three transmitters, respectively. Employing SIMO instead of MISO link configurations, enhanced performance gains of 4 dB and 5.5 dB have been achieved for two and three receivers, respectively. Reducing the distance to 500 m, a SNR of 19 dB was required for the SISO link configuration. Consequently, the performance gain was equal to 1 dB for the MISO link configurations either for two or three transmitters, whereas for the SIMO configurations, the performance gains were equal to 2.6 dB and 3.75 dB for two and three receivers, respectively. It has been proven that the use of spatial diversity by increasing the number of UV sources is not a panacea for further improvement of the energy efficiency and availability of UV links in the low to medium SNR range since the transmitters don't look at the same common atmospheric volume. Authors in [110] conducted an experimental study investigating a real-time NLOS UV system that operated at 265 nm along with an average power consumption equal to 10 mW (with its minimum power consumption being equal to 9.3 mW) and spatial diversity. In more detail, the system under investigation employed SIMO link configurations with up to four receivers and link length up to 35 m. Moreover, the average temperature was almost 25° , the average wind speed was equal to 12 km/h, and humidity was below 34%, while molecular distribution was almost invariable and the aerosol distribution was equal to 1200 per cm^3 . Under these conditions, the experimental UV system could achieve data rates at 64 kbps over 35 m link length with $\text{BER} = 10^{-6}$ when four receivers are utilized, while without diversity through consuming the same amount of power, BER was equal to 10^{-2} . Recently, the authors in [105], through the Gamma–Gamma turbulence model, along with the proposed maximal selective transmit diversity with the transmit power set to 20 dBm, i.e., 100 mW for a 200 m UV link, achieved $\text{BER} = 3 \times 10^{-12}$ and $\text{BER} = 5 \times 10^{-11}$ for weak and strong turbulent channels, respectively. In addition, the authors in [106], through the proposed time diversity technique for NLOS UV links operating at 260 nm, assessed the required power values to transmit at a wide range of average BER targets. Even in very strong turbulence, the SISO link (with no diversity) required 18 dBm, i.e., 63.1 mW for a target average $\text{BER} = 2 \times 10^{-10}$, while by employing time diversity, the virtual SIMO link transmitted power of 18 dBm, i.e., 63.1 mW could achieve an average $\text{BER} = 10^{-13}$, for 200 m propagation distance in all these link configurations.

Moreover, the tremendous progress in UV devices over the years has played a very crucial role in the deployment of more energy-efficient and performance-effective wireless links. To that end, in particular, the findings in [120–124] are interesting. Originally, the

authors in [121] utilized a 253 nm mercury-argon lamp created a UV link of 0.5 km length and by employed PPM to achieve a data rate of 10 kbps at $BER = 10^{-5}$, with a transmission power of 5 W. A few years later, the authors of [122] used a 265 nm mercury-xenon lamp and employed PPM to achieve a data rate of 1.2 Mbps over a UV link of 1.6 km, but with the required transmitted power equal to 25 W. With the advent of the first UV LEDs, after several years, the authors in [120] utilized LED arrays operating at 265 nm along with PPM and transmit power equal to 43 mW, to achieve a data rate equal to 5 kbps at a BER almost of 4×10^{-5} or 3×10^{-3} for a 10 m UV link with or without spatial diversity, respectively. The authors of [123] presented a UV system to achieve a data rate of 71 Mbps by utilizing QAM OFDM, and a 294 nm LED with transmit power of 190 μ W, as it was aligned with an avalanche photodiode (APD) at the receiver across a very short distance of 0.08 m. More recently, the authors in [124] used a 262 nm UV-C μ LED with a very low transmit power equal to 196 μ W to achieve a very high data rate of 800 Mbps or 1.1 Gbps at a BER equal to 3.8×10^{-3} at a short distance of 0.3 m, while utilizing OOK or OFDM, respectively. It is notable that this low optical power minimizes the adverse effects of UV light propagation in wireless communication systems. Considering the strong limitation of the commercial APD that was utilized at the receiver side, the very high achievable bit rates by a very low power consumption highlight the UV high performance and energy efficiency. It becomes evident that recent advances in UV equipment have enabled the establishment of these promising wireless links. Nevertheless, the need for extending UV link lengths remains a critical challenge.

In order to significantly extend UV link lengths, the potential of creating DF relay multi-hop UV configurations through a power-efficient modality has been investigated in [125–127]. The authors of [125] revealed the feasibility for establishing a multi-hop OOK NLOS UV link that could efficiently cover a propagation distance of 300 m by utilizing up to 10 hops, consuming 10 mW (1 mW per hop), and operating at 250 nm with a data rate of 64 kbps at a BER equal to 10^{-5} . In this respect, the authors of [126,127] demonstrated the feasibility of employing energy-efficient NLOS UV multi-hop links under weak to strong turbulence and utilizing the more sophisticated OFDM format, respectively. In general, an increment of the number of hops can ideally relax the power demand on individual relay nodes, which translates into dividing the total power to spaced relay nodes, each of which operates with much lower power consumption. The latter can be also be considered as an energy-efficient benefit in the coverage range extension by adjusting more relays, provided that each relay node obtains a fixed transmit power [125].

Table 2 below summarizes the background and evolution in UV communication era. In this respect, it visualizes a quick overview and comparison among UV communication systems in terms of significant performance metrics and technologies incorporated in the UV area. Additionally, Figure 2 shows the possibilities and energy-efficient applications of UV-C communication systems along with the limiting factors on their performance and energy consumption.

Table 2. UV communication systems.

Reference	Light Emitter	Turbulence Model	Modulation Technique	UV System Configuration	Diversity Method	Transmitted Power	Data Rate	Link Length	BER
[122]	Hg(Xe) lamp 265 nm	-	PPM	SISO	-	25 W	1.2 Mbps	1.6 km	-
[121]	Hg(Ar) lamp 253 nm	-	PPM	SISO	-	5 W	10 kbps	0.5 km	10^{-5}
[120]	UV LED arrays 265 nm	-	OOK/PPM	SISO	-	43 mW	5 kbps	10 m	8×10^{-3}
		-	OOK/PPM	MIMO	Spatial	43 mW	5 kbps	10 m	4×10^{-5}
[123]	UV LED 294 nm	-	OFDM	SISO	-	190 W	71 Mbps	0.08 m	3.8×10^{-3}
[124]	UV-C μ LED 262 nm	-	OFDM	SISO	-	196 μ W	1.1 Gbps	0.3 m	3.8×10^{-3}
[82]	UV LED 250 nm	-	OOK	SISO	-	50 mW	10 kbps	105 m	10^{-3}
		-	PPM	SISO	-	50 mW	10 kbps	155 m	10^{-3}

Table 2. Cont.

Reference	Light Emitter	Turbulence Model	Modulation Technique	UV System Configuration	Diversity Method	Transmitted Power	Data Rate	Link Length	BER
[110]	UV LED 265 nm	-	OOK OOK	SISO SIMO	- Spatial	10 mW 10 mW	64 kbps 64 kbps	35 m 35 m	10^{-2} 10^{-6}
[102]	UV LED 265 nm	LN (weak) LN (weak)	OOK 4-PPM	SISO SISO	- -	21.38 mW 12.59 mW	- -	50 m 50 m	10^{-5} 10^{-5}
[105]	UV LED 280 nm	G-G (weak) G-G (strong)	OOK OOK	SISO SISO	- -	100 mW 100 mW	- -	200 m 200 m	3×10^{-12} 5×10^{-11}
[106]	UV LED 260 nm	K (strong) K (strong)	OOK OOK	SISO SIMO	- Time	63.1 mW 63.1 mW	- -	200 m 200 m	2×10^{-10} 10^{-13}
[125]	UV Laser 250 nm	-	OOK	Multi-hop	-	10 mW	64 kbps	300 m	10^{-5}

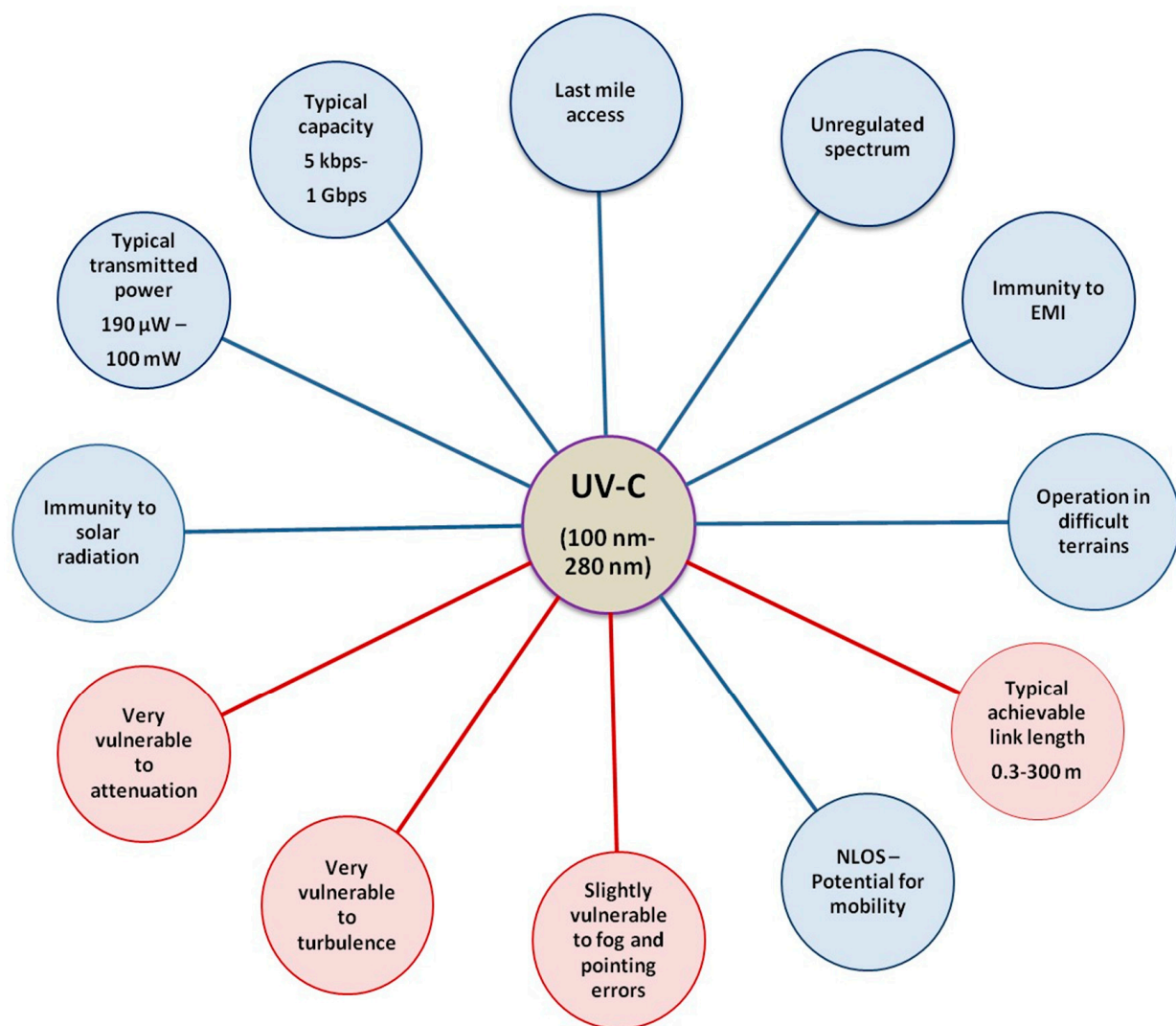


Figure 2. Possibilities and energy-efficient applications of UV-C communication systems, illustrated with blue color, versus adverse issues and limiting factors on their performance and energy consumption, illustrated with red color.

4. Transdermal Optical Wireless Communication

In numerous vital medical applications like neural recording and prostheses, there is a critical demand for high-capacity transmissions between an implanted medical device (IMD) and an out-of-body one. In order to record neural signals from internal devices and actuate them from external signals to guide prostheses, there is a need for even higher bit

rates along with lower power consumption to emulate the performance of human organs such as the cochlea. In these cases, human skin, in Greek derma, acts as a communication channel, and therefore this kind of communication is commonly known as transdermal communication. Nowadays, common modalities used for transdermal communication, which mainly rely on radio frequencies, cannot reach at the same time all the growing recent and future demands that mainly include wireless modality, remote control of the IMD, high noise and interference immunity, as well as communication with very high capacities along with very low power consumption. In this respect, tremendous recent progress in both medical and OWC fields has enabled the transition to the more bandwidth-effective and energy-efficient optical frequency spectrum, by establishing transdermal optical wireless (TOW) links. In basic terms, they are point-to-point wireless links that transmit the necessary data by means of light waves traversing through the skin. The light carrier is emitted by a proper LED or laser source and, after traveling inside the skin channel, it can be detected by a suitable photodiode at the receiver. Thus, through the utilization of an ultra-high frequency light carrier which can lead to an extremely-wide modulation bandwidth, we can guarantee the desirable high information capacity. At the same time, these links operate by consuming the desirable low power level for the medical implant. Another point in favor of TOW links is that they offer high-security level data transmissions, considering that the whole information is entailed within an extremely narrow light beam, which is very difficult to intercept. Moreover, contrary to their RF counterparts, they do not suffer from EMI or multi-path dispersion, and they are harmless to human health. Additionally, they operate with a low total cost within the unregulated optical spectrum, while due to their light weight and compactness, they are significantly flexible for installation and re-installation [10,128,129].

In view of the presented, several papers have been published devoted to TOW communication links. Among them, the feasibility of installing these links has been experimentally validated in [12,130–132]. In [131], the concept of a “Medical Spectral Window”, known also as “Therapeutic or Biological Optical Spectral Window”, has been experimentally proven, where radiation at wavelengths between 700 and 900 nm are least absorbed by the dominant absorbers in blood-perfused tissue, including hemoglobin and water. The good news is that there is compatibility with the first corresponding window for the wider optical communication transmissions, i.e., for wavelengths of 850 nm, where numerous optical sources operate. The latter enables the potential of power efficient and very rapid telemetry with medical implants. Within the appropriate medical issues near-IR spectral region, TOW link’s attenuation is minimized, and therefore the light obtains its maximum depth of penetration inside the skin [133,134], penetrating into the tissue up to some centimeters [130]. Consequently, within this medical optical window, we can achieve a specific transdermal propagation distance with the lowest amount of power consumption. On this basis, in [130], it has been revealed that TOW is a prime candidate for medical applications owing to its very low power consumption that is of order of μW or below 10 mW for extremely high capacities, while their RF counterparts need some tens of mW to operate. Thus, while a high speed RF transdermal link of 24 Mbps has been recently achieved in [135], it required a relatively large power of 30 mW. On the other hand, via TOW links in [129], by utilizing a vertical cavity surface emitting laser (VCSEL) with 850 nm wavelength, a TOW link achieving 50 Mbps through adequately thick tissue with power consumption only of 4.1 mW or less was reported in [132]. Additionally, in vivo experiments carried out on an anesthetized sheep revealed the potential of transmitting data at 100 Mbps consuming only 2.1 mW. Next, the authors in [136] established a bi-directional TOW system using a visible light and near infrared in downlink and uplink, respectively. By conducting in vitro experiments on a 2 mm porcine skin channel, they achieved 1 and 100 Mbps data rates by consuming 29 μW and 3.2 mW in downlink and uplink, respectively. Recently, significant progress has been carried out in cochlear implants for the hearing impaired. Toward this direction, the authors in [137] introduced a TOW-based communication system architecture which has been proven to be capable of significantly improving the reliability

along with the spectral and power efficiency of the TOW link in cochlear IMDs. It has been shown that for a 8 mm transdermal link, an increase in the transmission power spectral density (PSD) from 0.001 $\mu\text{W}/\text{MHz}$ to 0.01 $\mu\text{W}/\text{MHz}$ caused a 56.5% increase in the corresponding spectral efficiency. Note that even in the worst case scenario, where the skin thickness was increased to 10 mm, along with a very low transmission signal PSD of about 10^{-4} $\mu\text{W}/\text{MHz}$, a spectral efficiency in the order of 8 bits/channel use has been achieved. Very recently, the authors of [138] introduced an all-optical cochlear implant architecture in an attempt to directly convert acoustic to optical signals capable of stimulating the cochlear neurons toward the direction to restore hearing to hearing-impaired people. Their findings demonstrated that for optical transmission power of less than 10 mW, the probability of hearing was evaluated at least equal to 50% for 4–8 mm skin thicknesses. On the other hand, the probability of neural damage was found to be defined for extremely high optical transmission power values, i.e., higher than 1 W. Even in a skin thickness of 7 mm, an almost certain damage of acoustic nerve has been shown to require a transmit power of 2 W. In short, power consumption is a very vital factor for TOW links because it is directly related to the operational lifetime of the implanted devices, which in some cases, translates into patient's longevity, whereas consuming more power than the pre-defined thresholds may cause damage to human health.

Despite the encouraging and impressive results, human skin is a very complex, multi-layer, strongly anisotropic biological structure that comprises many and different constituents and characteristics that depend heavily on variable and random conditions, such as skin's thickness, different tissues, topology, region, age, race, gender, and age. Light propagating through the skin is reflected, scattered, and absorbed by all its constituents [131]. By choosing a proper light wavelength from the medical spectral window, we can minimize the effects of absorption for TOW links, which still suffer from significant photon scattering. Indeed, within this wavelength window, only 10–30% of incident optical power is transmitted via typically thick (2–6 mm) skin channels when the laser and the detector aperture are aligned [131,133]. Even in perfect alignments between source and receiver aperture, in order to increase the received signal level in order to overcome scattering, one should resort to a large size photodetector. Larger photodiodes result in a limited bandwidth [8], which brings about lower capacities. Hence, the researchers aim to maintain a balance between power consumption, achievable capacity, photodetector's size, and skin thickness.

In several papers on TOW, researchers reported the pointing errors effect due to the unavoidable patient's movements, which is another significant issue. This issue has been either neglected or it has been assessed by deterministic models that are less realistic for their description. Only in [137,138], the stochastic nature of pointing errors has been taken into account. This concept has been first reported in [139], and then in [140–142], where the authors modeled the pointing errors effect relying on the zero boresight Rayleigh distribution model [44], which has been extensively used in the wider optical wireless communications area. For a power spectral density of 0.1 $\mu\text{W}/\text{Hz}$, they showed that for the initial millimeters of in-body propagation distance, pointing errors may dominate skin-induced attenuation being the major performance limiting factor, whereas after 5 to 6 mm, skin-induced attenuation dominates. In [3,143], the more generalized NZB pointing errors model was proposed, as well the diversity method was introduced in the TOW area with the intention to overcome the combined influence of skin-induced attenuation and stochastic generalized pointing errors. For a power spectral density of 1 mW/Hz and a reasonable use of spatial or time diversity, they achieved in [143] the outage probability of 10^{-6} for 8 mm skin thickness, as well as in [3] under strong NZB misalignments, they achieved an ABER of 8×10^{-7} by utilizing the more power-effective 8-PPM than OOK format for further outage performance improvements. However, experimental works need to be conducted to further verify this energy-efficient approach.

Apart from the direct TOW link configurations that comprise the transmitter, the skin-channel and the receiver, retro-reflective link configurations are alternatively used. Specifically, in the former configurations, a light source conveys data from inside the body

to an external receiver, and thus the optic signals pass through the skin channel at once, while in the latter, light emitted from an external, continuous wave light source is retro-reflected by a device inside the body. Thus, through retro-reflective TOW transmissions, only retro-reflector needs to be implanted since both the transmitter and receiver are out of the body. Appropriate signal models of both configurations were introduced in [130], where the feasibility of both configurations was also demonstrated assuming intensity modulation/direct detection (IM/DD) with OOK modulation format, and achieving 0.4 μW and 4 mW transmissions power at a BER = 10^{-6} for direct and retro-reflective TOW links. The authors in [5] utilized a continuous wave laser operating at 854.52 nm with a low transmit power of 2.9 mW along with an electro absorption modulator at the retro-reflector side and a 4 cm² skin sample of a 10 months old laboratory rat to prove the feasibility of established real retro-reflective TOW links. The authors of [144,145], for a power spectral density of 1 $\mu\text{W}/\text{MHz}$, presented encouraging ABER results of 10^{-5} to 10^{-4} for a reasonable use of wavelength and spatial diversity configurations. Bearing in mind that the most demanding medical applications with IMDs require a signal power density spectrum from 1 $\mu\text{W}/\text{MHz}$ to 20 $\mu\text{W}/\text{MHz}$, the authors in [145] showed that over this power density spectrum region, they achieved the proper average SNR values, which were required to drastically address the major effects that degrade TOW performance. Additional experimental work is needed for retro-reflective TOW systems in order to play a key role in energy-efficient wireless telemetry with medical implants.

Recently, the concept of simultaneous light-wave information and power transfer (SLIPT) has been presented in [146]. Employing this method, IMDs have the potential to both harvest energy and, at the same time, communicate. SLIPT has the potential to significantly prolong the IMD's lifetime as well as to lead to a more energy-efficient TOW communication. In this respect, SLIPT is ideally suited for sophisticated applications of real-time and interactive communication between the in-body and out-of-the body world. Bearing in mind that the received photocurrent has both alternative current (AC) and direct current (DC) components, the main concept of SLIPT is to split it into AC and DC, which will be respectively utilized for information decoding and energy harvesting. The latter can be implemented by means of signal component separation receiver architecture, where in order to split the arriving signal in DC and AC components, we utilize an inductor and a capacitor at energy harvester and information decoder branches outputs, respectively. Alternatively, by utilizing a proper diode instead of the inductor, time splitting-switching technique could be used in which the receiver switches in time between the modes of information decoding and energy harvesting or even to utilize multiple photoelectric converters at the receiver's input. The former signal component separation receiver architecture is capable of achieving higher energy harvesting efficiency in comparison with time switching architecture, since it simultaneously realizes energy harvesting and information decoding without wasting the DC component for the sake of information decoding [147]. Nevertheless, SLIPT method remains to be practically implemented in the near future for real TOW communication and energy-efficient links.

Table 3 below summarizes the performance comparison between conventional RF and the emerged TOW communication links with IMDs in terms of energy efficiency, transmission speed, and robustness. It also provides a quick overview of the evolution of these direct TOW communication links.

Table 3. SISO direct transdermal wireless communication links.

Reference	Type	Transmitted Power	Data Rate	Skin Thickness	Deterministic Misalignment	BER
[135]	RF	30 mW	24 Mbps	-	-	-
[148]	RF-IR	90 mW	80 Mbps	3 mm	2 mm	10^{-14}
[149]	RF (cochlear)	20–40 mW	1 Mbps	4–10 mm	-	-
[134]	TOW	16 mW	16 Mbps	4 mm	2 mm	10^{-9}
[129]	TOW	4.1 mW	50 Mbps	4 mm	2 mm	10^{-5}
[150]	TOW	2.8 mW	75 Mbps	6 mm	4 mm	10^{-5}
[151]	TOW (retinal)	190–270 μ W	2–3 Mbps	300 μ m	-	-
[132]	TOW (in vivo)	2.1 mW	100 Mbps	2.5 mm	-	2×10^{-7}
[137]	TOW (cochlear)	2–10 μ W	150–160 Mbps	4–10 mm	-	-
[137]	TOW	PSD = 0.1 μ W/MHz	128.77 Mbps	5 mm	-	-
	cochlear	10 MHz, $\theta = 15^\circ$	119.43 Mbps	10 mm	-	-
[137]	TOW	PSD = 1 μ W/MHz	207 Mbps-	4 mm	-	-
	cochlear	13–20 MHz	325 Mbps	-	-	-
[136]	TOW bi-directional	290 μ W 3.2 mW	1 Mbps (down) 100 Mbps (up)	2 mm	-	-

Table 4 below provides a quick overview of the potential of establishing either SISO or SIMO OOK TOW R-R links in contradistinction to direct OOK TOW link configurations. Additionally, Figure 3 presents the possibilities and energy-efficient applications of TOW communication systems along with the limiting factors on their performance and energy consumption.

Table 4. TOW systems with SISO and/or SIMO retro-reflective (R-R) links.

Reference	TOW System Configuration	Transmitted Power	Skin Thickness	Pointing Errors	BER	Outage Probability
[130]	SISO/direct	0.4 μ W	1 mm	-	$\cong 10^{-6}$	-
	SISO/R-R	4 mW	1 mm	-	$\cong 10^{-6}$	-
[5]	SISO/R-R	2.9 mW	1 mm	-	-	-
[145]	SISO/R-R	1 μ W/MHz	8 mm	ZB	$\cong 3 \times 10^{-4}$	-
	SIMO/R-R	1 μ W/MHz	8 mm	NZB	$\cong 8 \times 10^{-7}$	-
[144]	SISO/R-R	1 μ W/MHz	7 mm	ZB	-	$\cong 2.3 \times 10^{-2}$
	SIMO/R-R	1 μ W/MHz	7 mm	NZB	-	$\cong 10^{-5}$

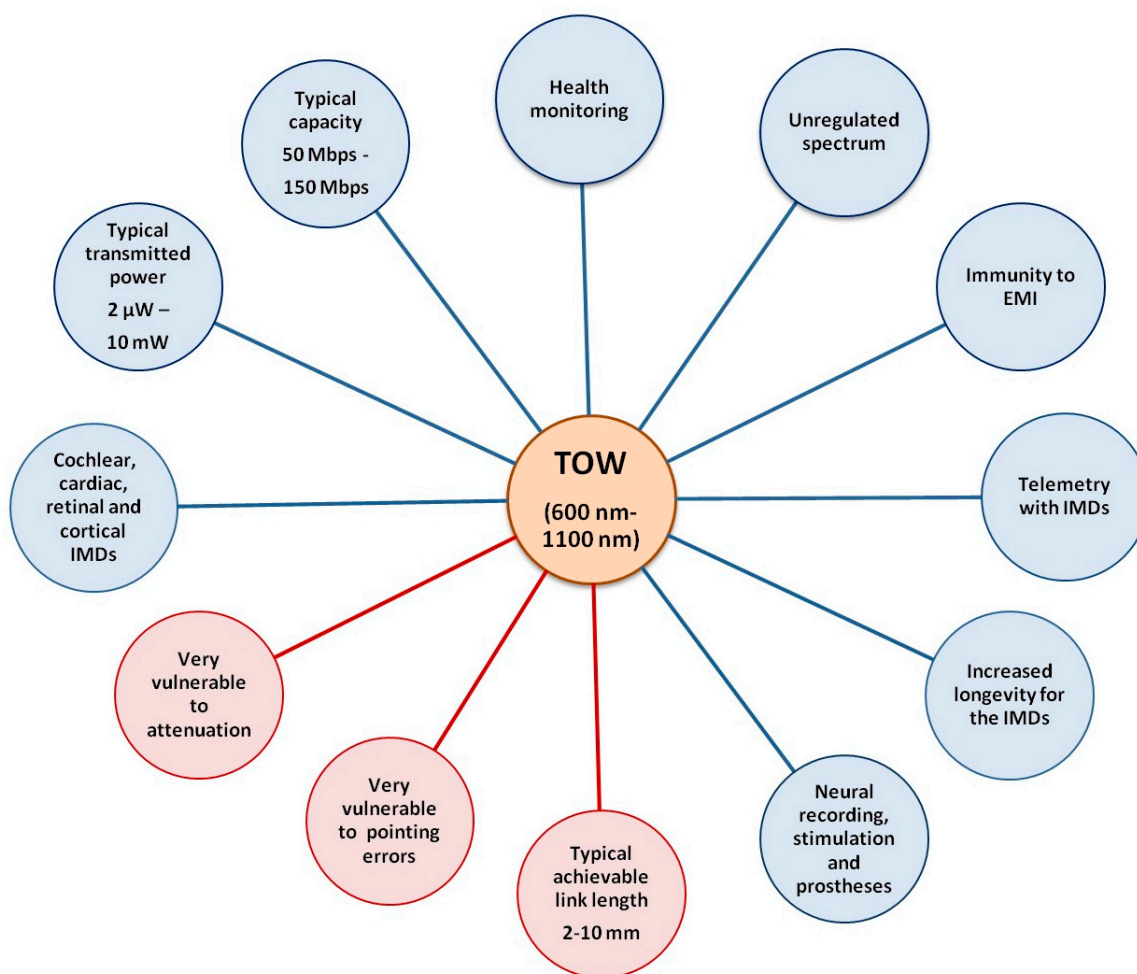


Figure 3. Possibilities and energy-efficient applications of TOW communication systems, illustrated with blue color, versus adverse issues and limiting factors on their performance and energy consumption, illustrated with red color.

5. Discussion

In Table 1, in the first four rows, i.e., in [68–71], the potential of establishing practical high speed and robust FSO links with low power consumption is highlighted. Indeed, in the third row, in [70], by transmitting only 4 mW and even by utilizing the less sophisticated but simplest OOK modulation format, a FSO link of 2.5 Gbps data rate has been achieved at a BER target below 10^{-9} covering a propagation distance of 2.7 km. This impressive performance by means of both energy efficient and robust high-speed transmission is comparable to that of optical fiber systems, i.e., they outperform significantly in comparison to their conventional RF wireless counterparts. The latter also indicates the potential of combining FSO with optical fiber systems, which is further highlighted in [69,71], through the use of WDM technique which results in achieving the extremely high data rates of 1.28 Tbps and 2.2 Tbps at BER targets of 10^{-9} and 10^{-6} , respectively. Next, in the fifth row, in [26], the performance comparison between the two different scenarios depicted for the investigated FSO link (clear sky versus fog) demonstrate that fog degrades ergodic capacity, and thus maximum average data rate, as well as increases BER for the same acceptable amount of transmitted power. The latter implies that even in adverse fog effects, typical FSO link lengths up to several hundred meters can be achieved through an adequate energy-efficient manner. Next, in sixth and seventh rows, i.e., in [72,73], the potential of establishing practical energy-efficient coastal FSO links is visualized for short (70 m) to long (2958 m) propagation distances, respectively. As it was expected, the shorter link needs less power consumption. Increasing the distance from 70 to 2958 m, a reasonable larger amount of

transmitted power is needed to address the emergence of turbulence along with attenuation due to the larger propagation distance through the coastal channel. Nevertheless, both the increase in power consumption and the decrease in data rate are acceptable for the achievement of this large propagating distance through a coastal environment.

The next four rows in Table 1 are focused on different link realizations of the investigated 1 km FSO link in [2]. Among them, the first row illustrates that the diversity method guarantees more robust FSO transmissions in a very energy-efficient manner. Indeed, by consuming the same desirable amount of 14.125 mW, we achieve an ABER reduction from 2.2×10^{-3} to 3×10^{-5} when spatial diversity is implemented. Specifically, we can achieve the same ABER target value of a SISO FSO link by reducing the transmitted power, provided that diversity techniques are employed. Note also that both turbulence-induced and misalignment-induced fading have been considered. Specifically, for SISO link configurations, i.e., without spatial diversity, zero boresight pointing (ZB) errors can be considered without a loss of generality, whereas for SIMO link configurations, i.e., with spatial diversity, the non-zero boresight (NZB) pointing errors components should also be taken into account due to the unavoidable distance between receiver apertures. The following row referred to in [2], compared with its previous first one, reveals the impact of turbulence effect. Indeed, by consuming the same energy under the same link characteristics but through a weak turbulence instead of strong, even more decreased ABER values are achieved for SISO link, and much less for SIMO link configuration. The third row referred to in [2], illustrates that PPM, and more precisely 8-PMM format, is more energy efficient than OOK, since for the same transmitted power, it can reduce ABER from 10^{-3} to 10^{-4} under the presence of strong NZB pointing errors. Additionally, in the fourth row, NZB pointing errors are getting weak, and thus better ABER results are depicted, especially when 8-PMM format is utilized.

The penultimate row in Table 1, which refers to [64], indicates the potential of extending the FSO propagation distance through the use of DF relays at a reasonable and acceptable expense of energy and outage performance cost. As we can see, by transforming the single-hop to a dual-hop FSO link by means of employing a DF relay node, we need to increase the transmitted power from 14.125 mW to 28.25 mW with an additional increase in ASEP from 1.5×10^{-3} to 2.9×10^{-3} . The latter is acceptable, considering also that through dual-hop configuration, the total link length has been doubled from 1 km to 2 km. Finally, the last row in Table 1 which refers to [65], demonstrates that under certain circumstances, the GVD effect can be treated as a key contributor to establishing more robust and energy efficient links. In fact, it is illustrated that by adjusting $C < 0$, i.e., by emitting negative chirped initial short pulses with the same acceptable power, we create GVD-induced narrowing propagating pulses for some initial propagation distance, which ultimately leads to a decrease in the probability of fade (Pf) from 3×10^{-3} to 2×10^{-3} for the total FSO link. It is recalled that the probability of fade represents the probability that the normalized irradiance arriving at the receiver is lower than the receiver's threshold, which guarantees the appropriate operation of the link [65]. Nevertheless, bearing in mind that GVD is highly distant dependent on atmospheric dispersive channels, the total link distance should be large enough, i.e., several km (10 km as illustrated, for example, in the final row) in order to practically take advantage of the beneficial GVD impact.

The first two rows in Table 2, which are referred to in [121,122], consist the initial significant efforts of establishing UV communication links, which have been reported in the open UV literature. It becomes evident that although they could cover relatively long propagation distances along with promising data rates, the very high required transmitted power values of 5 W and 25 W made them energy inefficient, even by employing the inherent energy-efficient PPM scheme. As it can be inferred from the first two rows, this problem arises from the utilized light sources that existed in that time. Indeed, with the advent of more energy-efficient UV light sources and devices, this problem has been significantly overcome, even if only to a relatively limited coverage area, as it becomes evident from the transmitted power column comparison between the first two rows ver-

sus the rest of the rows in Table 2. More precisely, the third row that refers to [120] requires 43 mW by means of the use of UV LED arrays and reduces BER to 4×10^{-5} from 8×10^{-3} , when spatial diversity through UV MIMO links is utilized. In this context, the third row illustrates that as in the case with IR FSO, the diversity method can be also used as an energy-efficient contributor for the establishment of more robust UV communication systems. This beneficial impact of spatial diversity can be also observed in the seventh row, where UV SIMO links have been created through spatial diversity. The fourth row and the fifth row which refer to [123,124], respectively both utilize the more sophisticated OFDM format and consume only 190 μ W and 196 μ W, i.e., almost the same power to achieve the impressive data rates of 71 Mbps and 1.1 Gbps, respectively at the same BER = 3.8×10^{-3} for 0.08 m and 0.3 m, respectively. Consequently, it is observed that although the latter has a larger link length, it achieves a higher data rate at the same BER than the former. This is because the latter utilizes a more sophisticated UV-C μ LED technology. In the sixth row that refers to [82], the beneficial impact on the energy consumption of UV communication links is highlighted when utilizing PMM instead of OOK. Indeed, for both OOK and PPM UV link realizations, by consuming 50 mW for a data rate of 10 kbps at the same BER target of 10^{-3} , the achievable UV link length for OOK is equal to 105 m, whereas for PPM, the achievable UV link length increases to 155 m. It becomes therefore evident that in order to achieve the target of 155 m with OOK, a larger amount of transmitted power consumption, i.e., larger than 50 mW is needed which denotes that OOK is less power effective than PPM. The latter is also observed in the eighth row which refers [102], and indicates that under the same LN-modeled weak turbulent channel, the investigated 50 m UV link achieves a BER equal to 10^{-5} with the required transmitted power being 21.38 mW or even better 12.59 mW by utilizing OOK or 4-PPM formats, respectively. In the ninth row, which corresponds to [105], the Gamma–Gamma (G–G) turbulence model has been introduced in UV-C regime to describe weak to strong turbulence-induced UV irradiance scintillations. It is revealed that by consuming 100 mW for the operation of a 200 m UV link, the achievable BER increases from 3×10^{-12} to 5×10^{-11} from weak to strong turbulence conditions, respectively. Consequently, the turbulence effect plays a key role in the energy efficiency and outage performance of typical UV links. More recently, in the penultimate row in Table 2, which refers to [106], the more compact K-distribution model has been introduced in the UV area along with the time diversity technique. The former has been proven to be accurate for strong turbulence conditions, while the latter has been proven to be a useful tool to address these strong turbulence-induced UV irradiance scintillations in an attempt to create more robust and energy-efficient UV systems. As a result, by consuming 63.1 mW to cover a distance of 200 m, an average BER is equal to 10^{-13} or 2×10^{-10} with or without time diversity, respectively. The ultimate row in Table 2 that describes [125], depicts the potential of extending UV link by means of establishing intermediate, serially connected DF relay nodes, i.e., through multi-hop UV link configurations. By consuming only 10 mW for the total multi-hop UV link (1 mW is devoted to each of the ten hops of the total link that stem from the nine serially connected intermediate DF relay nodes), a total propagation distance of 300 m has been eventually achieved, which is adequately large for typical UV communication links.

The first three rows in Table 3 which are devoted to [135,148,149], depict traditional transdermal link configurations that utilize RF, which are nowadays the common technology for communications with IMDs, whereas the rest of the rows in Table 3 refer to their promising TOW alternative. Specifically, they refer to direct TOW links with OOK, which is to date the only modulation scheme that has been implemented for practical TOW links. At first glance, we can realize that TOW offers higher data rates consuming at the same time less energy. It is also clarified here that despite the efforts depicted in the first three rows for RF, and even by combining RF with IR as reported in the second row, 50 Mbps will be required when 100 channels of neural waveform data are recorded simultaneously [148]. Nevertheless, even 20 mW remains as a large amount of power consumption for IMDs, since the corresponding target is up to 10 mW [3,11]. Therefore, it becomes evident that

none of the transdermal wireless RF based implementations can reach these growing energy consumption and capacity demands. Contrary to RF, the rest of the rows in Table 3 show that TOW can achieve them. The latter is emphasized in the seventh row that refers to [132] for general transdermal applications, which require wireless communication with IMDs. It is shown that by consuming only 2.1 mW, an in vivo TOW link achieved 100 Mbps through a skin thickness of 2.5 mm at an adequate BER target of 2×10^{-7} . Additionally, of particular interest is the specific case of transdermal wireless communication with cochlear IMDs. The performance comparison between the third and eighth row in Table 3 that refers to RF [135], and TOW communication with cochlear IMDs [137], respectively reveals that by operating both at the same regime of skin thickness, the former needs 20–40 mW to provide 1 Mbps, while the latter needs only 2–10 μ W to provide remarkable data rates of 150 Mbps and 160 Mbps, respectively. Therefore, it becomes clear that TOW communication with cochlear IMDs outperforms its RF counterpart in terms of both energy efficiency and capacity. Additionally, the tenth row that also refers to [137] indicates that by practically consuming less power, i.e., equal to 1 mW (PSD = 0.1 μ W/MHz denotes the power spectral density with 10 MHz being the available bandwidth) along with a divergence angle $\theta = 15^\circ$, it still achieves impressive data rates of 128.77 Mbps and 119.43 Mbps for 5 mm and 10 mm skin thickness, respectively. Note that a skin thickness of up to 10 mm is considered to be adequate for cochlear IMDs. In this context, the eleventh row that refers once again to [137], demonstrates the feasibility of enhancing even more the capacity of cochlear TOW communication links in a very energy efficient way. In more detail, by increasing both PSD = 1 μ W/MHz and available bandwidth in the frequency region of 13–20 MHz, even higher data rates have been achieved, i.e., 207 Mbps and 325 Mbps, respectively provided that the skin thickness has been equal to 4 mm. Finally, in the last row in Table 3 that refers to [136], the potential of establishing bi-directional TOW links has been proven. Indeed, it has been shown that for a skin channel of 2 mm thickness, by consuming only 290 μ W and 3.2 mW for the downlink and the uplink, 1 Mbps and 100 Mbps data rates have been achieved, respectively.

The first rows in Table 4 which refer to [130], demonstrate the feasibility of establishing R-R TOW links as a viable alternative to direct TOW link configurations. In more detail, at the same BER target and the at same skin thickness, although direct SISO TOW configuration outperforms R-R SISO TOW configuration in terms of energy consumption due to the fact that via direct SISO TOW the light traverses the skin channel at once and not at twice as in the case with SISO R-R TOW configuration, the SISO-RR TOW link still needs power consumption of 4 mW which is acceptable, as well. Next, in the second row that refers to [5], an even more energy-efficient SISO R-R TOW link configuration has been achieved by consuming 2.9 mW through the utilization of a more sophisticated and energy-efficient implanted device. Nevertheless, it still exceeds the power consumption of 0.4 μ W that required a direct TOW link in the first row, i.e., in [130]. In the third and in the last row, i.e., in [145] and in [144], respectively, diversity techniques have been introduced in the R-R TOW area in an attempt to enhance energy efficiency for the more robust TOW R-R systems that emerge via the use of diversity. In the third row, i.e., in [145], SISO and SIMO RR TOW link configurations have been investigated. Note that SISO implies that there is no diversity, while SIMO configurations have been realized through the use of spatial diversity. For an acceptable PSD, as it has been explained above, of 1 μ W/MHz (typically for an available bandwidth of 10 MHz) and at the same skin-channel thickness of 8 mm, SISO R-R TOW link achieved an average BER at 3×10^{-4} , while SIMO RR-TOW system achieved a significantly decreased average BER at 3×10^{-7} , taking also into consideration the stochastic nature of ZB and NZB pointing errors, respectively. The latter demonstrates that spatial diversity can enhance the ABER performance of TOW RR links in a power-efficient mode. In the same context, in the last row, i.e., in [144], it is illustrated that by using SIMO R-R TOW instead of SISO R-R TOW, the total outage probability has been impressively decreased, almost from 2.3×10^{-2} to 10^{-5} . Note that in [144], wavelength diversity has been utilized

to create the SIMO R-R TOW system. Therefore, in any case, diversity enhances the outage performance of R-R TOW links with an acceptable power level.

6. Conclusions

This article has presented an overview of three distinct optical wireless communication technologies, i.e., terrestrial free-space optical communication for outdoor application, ultraviolet wireless communication, and transdermal optical wireless communication, highlighting their potential to reach the growing, and at the same time, urgent demand of establishing high quality and energy-efficient communication services in line with environmental and human health protection. To this end, we focused on their low power consumption potential and implementations. The major effects and critical limiting factors that impede this development have been described as well as methods, techniques, and architectures that seem to be capable of drastically addressing their detrimental impact. It is notable that some of them have been already emerged in the commercial field, while the rest are very promising candidates to be adopted in many applications in the near future. Moreover, the presented technologies can be incorporated as complementary technologies to the existing conventional ones to alleviate their high energy consumption and enhance their performance. Alternatively, they can cooperate between themselves in establishing even more energy-efficient and performance-effective full optical wireless networks.

Funding: This research was funded by Ajman University, grant number 2022-IRG-ENIT-19.

Acknowledgments: G.K.V. and K.A. acknowledge funding from Ajman University under grant agreement 2022-IRG-ENIT-19.

Conflicts of Interest: The authors declare no conflict of interest.

References

1. Yücel, M.; Açıkgöz, M. Optical Communication Infrastructure in New Generation Mobile Networks. *Fiber Integr. Opt.* **2023**, *42*, 53–92. [[CrossRef](#)]
2. Varotsos, G.K.; Nistazakis, H.E.; Petkovic, M.I.; Djordjevic, G.T.; Tombras, G.S. SIMO Optical Wireless Links with Nonzero Boresight Pointing Errors over M modeled Turbulence Channels. *Elsevier Opt. Commun.* **2017**, *403*, 391–400. [[CrossRef](#)]
3. Varotsos, G.K.; Nistazakis, H.E.; Aidinis, K.; Jaber, F.; Rahman, K.K. Transdermal Optical Wireless Links with Multiple Receivers in the Presence of Skin-Induced Attenuation and Pointing Errors. *Computation* **2019**, *7*, 33. [[CrossRef](#)]
4. Celik, A.; Romdhane, I.; Kaddoum, G.; Eltawil, A.M. A top-down survey on optical wireless communications for the internet of things. *IEEE Commun. Surv. Tutor.* **2022**, *25*, 1–45. [[CrossRef](#)]
5. Abualhoul, M.Y.; Svenmarker, P.; Wang, Q.; Andersson, J.Y.; Johansson, A.J. Free space optical link for biomedical applications. In Proceedings of the 2012 Annual International Conference of the IEEE Engineering in Medicine and Biology Society, San Diego, CA, USA, 28 August–1 September 2012.
6. Khalighi, M.A.; Uysal, M. Survey on free space optical communication: A communication theory perspective. *IEEE Commun. Surv. Tutor.* **2014**, *16*, 2231–2258. [[CrossRef](#)]
7. Anandkumar, D.; Sangeetha, R.G. A survey on performance enhancement in free space optical communication system through channel models and modulation techniques. *Opt. Quantum Electron.* **2021**, *53*, 5. [[CrossRef](#)]
8. Ghassemlooy, Z.; Arnon, S.; Uysal, M.; Xu, Z.; Cheng, J. Emerging optical wireless communications—advances and challenges. *IEEE J. Sel. Areas Commun.* **2015**, *33*, 1738–1749. [[CrossRef](#)]
9. Vavoulas, A.; Sandalidis, H.G.; Chatzidiamantis, N.D.; Xu, Z.; Karagiannidis, G.K. A survey on ultraviolet C-band (UV-C) communications. *IEEE Commun. Surv. Tutor.* **2019**, *21*, 2111–2133. [[CrossRef](#)]
10. Ritter, R.; Handwerker, J.; Liu, T.; Ortmanns, M. Telemetry for implantable medical devices: Part 1—media properties and standards. *IEEE Solid-State Circuits Mag.* **2014**, *6*, 47–51. [[CrossRef](#)]
11. Varotsos, G.K.; Nistazakis, H.E.; Aidinis, K.; Jaber, F.; Rahman, K.K.M. Transdermal subcarrier L-PSK or DBPSK optical wireless links with time diversity, skin attenuation and spatial jitter. *J. Mod. Opt.* **2020**, *67*, 1233–1240. [[CrossRef](#)]
12. Liu, T.; Anders, J.; Ortmanns, M. System level model for transcutaneous optical telemetric link. In Proceedings of the 2013 IEEE International Symposium on Circuits and Systems (ISCAS), Beijing, China, 19–23 May 2013.
13. Taherkhani, M.; Sadeghzadeh, R.A.; Kashani, Z.G. Attenuation analysis of THz/IR waves under different turbulence conditions using gamma-gamma model. In Proceedings of the Electrical Engineering (ICEE), Iranian Conference on, Sadjad University of Technology, Mashhad, Iran, 8–10 May 2018; IEEE: Piscataway, NJ, USA; pp. 424–428.
14. Chaudhary, S.; Amphawan, A. The role and challenges of free-space optical systems. *J. Opt. Commun.* **2014**, *35*, 327–334. [[CrossRef](#)]

15. Sangeetha, R.G.; Hemanth, C.; Jaiswal, I. Performance of different modulation scheme in free space optical transmission—A review. *Optik* **2022**, *254*, 168675. [[CrossRef](#)]
16. Drost, R.J.; Sadler, B.M. Survey of ultraviolet non-line-of-sight communications. *Semicond. Sci. Technol.* **2014**, *29*, 084006. [[CrossRef](#)]
17. Kiourti, A.; Psathas, K.A.; Nikita, K.S. Implantable and ingestible medical devices with wireless telemetry functionalities: A review of current status and challenges. *Bioelectromagnetics* **2014**, *35*, 1–15. [[CrossRef](#)]
18. Al-Gailani, S.A.; Salleh, M.F.M.; Salem, A.A.; Shaddad, R.Q.; Sheikh, U.U.; Algeelani, N.A.; Almohamad, T.A. A survey of free space optics (FSO) communication systems, links, and networks. *IEEE Access* **2020**, *9*, 7353–7373. [[CrossRef](#)]
19. Mansour, A.; Mesleh, R.; Abaza, M. New challenges in wireless and free space optical communications. *Opt. Lasers Eng.* **2017**, *89*, 95–108. [[CrossRef](#)]
20. Farooq, E.; Sahu, A.; Gupta, S.K. Survey on FSO communication system—Limitations and enhancement techniques. In *Optical and Wireless Technologies: Proceedings of OWT 2017*, 1st ed.; Janyani, V., Tiwari, M., Singh, G., Minzioni, P., Eds.; Springer: Singapore, 2018; Volume 472, pp. 255–264.
21. Burton, A.; Le Minh, H.; Ghassemlooy, Z.; Bentley, E.; Botella, C. Experimental Demonstration of 50-Mb/s Visible Light Communications Using 4×4 MIMO. *IEEE Photonics Technol. Lett.* **2014**, *26*, 945–948. [[CrossRef](#)]
22. Ghassemlooy, Z.; Popoola, W.O. Terrestrial free-space optical communications. In *Mobile and Wireless Communications: Network Layer and Circuit Level Design*; InTech: London, UK, 2010; pp. 355–392.
23. Majumdar, A.K. Free-space laser communication performance in the atmospheric channel. *J. Opt. Fiber Commun. Rep.* **2005**, *2*, 345–396. [[CrossRef](#)]
24. Varotsos, G.K.; Nistazakis, H.E.; Stassinakis, A.N.; Volos, C.K.; Christofilakis, V.; Tombras, G.S. Mixed Topology of DF Relayed Terrestrial Optical Wireless Links with Generalized Pointing Errors over Turbulence Channels. *Technologies* **2018**, *6*, 121. [[CrossRef](#)]
25. Varotsos, G.K.; Nistazakis, H.E.; Tombras, G.S. OFDM RoFSO Links with Relays Over Turbulence Channels and Nonzero Boresight Pointing Errors. *J. Commun.* **2017**, *12*, 644. [[CrossRef](#)]
26. Esmail, M.A.; Fathallah, H.; Alouini, M.S. Outdoor FSO communications under fog: Attenuation modeling and performance evaluation. *IEEE Photonics J.* **2016**, *8*, 1–22. [[CrossRef](#)]
27. Majumdar, A.K.; Ricklin, J.C.; Leitgeb, E.; Gebhart, M.; Birnbacher, U. Optical networks, last mile access and applications. In *Free-Space Laser Communications: Principles and Advances*; Springer: New York, NY, USA, 2008; Volume 2, pp. 273–302.
28. Leitgeb, E.; Awan, M.S.; Brandl, P.; Plank, T.; Capsoni, C.; Nebuloni, R.; Nebuloni, R.; Javornik, T.; Kandus, G.; Sheikh Muhammad, S.; et al. Current optical technologies for wireless access. In Proceedings of the 2009 10th International Conference on Telecommunications, Zagreb, Croatia, 8–10 June 2009.
29. Awan, M.S.; Capsoni, C.; Leitgeb, E.; Nebuloni, R.; Nadeem, F.; Khan, M.S. FSO-relevant new measurement results under moderate continental fog conditions at Graz and Milan. In Proceedings of the 2008 4th Advanced Satellite Mobile Systems, Bologna, Italy, 26–28 August 2008.
30. Alkholidi, A.; Altowij, K. Effect of clear atmospheric turbulence on quality of free space optical communications in Western Asia. In *Optical Communications Systems*, 1st ed.; Narottam, D., Ed.; InTech: Rijeka, Croatia, 2012; Volume 1, pp. 41–75.
31. Kim, I.I.; Korevaar, E.J. Availability of free-space optics (FSO) and hybrid FSO/RF systems. In *Optical Wireless Communications IV*; SPIE: Bellingham, WA, USA, 2001; Volume 4530, pp. 84–95.
32. Zhu, X.; Kahn, J.M. Free-space optical communication through atmospheric turbulence channels. *IEEE Trans. Commun.* **2002**, *50*, 1293–1300.
33. Varotsos, G.K.; Nistazakis, H.E.; Stassinakis, A.N.; Tombras, G.S.; Christofilakis, V.; Volos, C.K. Outage performance of mixed, parallel and serial DF relayed FSO links over weak turbulence channels with nonzero boresight pointing errors. In Proceedings of the 2018 7th International Conference on Modern Circuits and Systems Technologies (MOCASST), Thessaloniki, Greece, 7–9 May 2018.
34. Killinger, D. Free space optics for laser communication through the air. *Opt. Photonics News* **2002**, *13*, 36–42. [[CrossRef](#)]
35. Al-Habash, M.A.; Andrews, L.C.; Phillips, R.L. Mathematical model for the irradiance probability density function of a laser beam propagating through turbulent media. *Opt. Eng.* **2001**, *40*, 1554–1562. [[CrossRef](#)]
36. Stassinakis, A.N.; Nistazakis, H.E.; Varotsos, G.K.; Tombras, G.S.; Tsigopoulos, A.D.; Christofilakis, V. Outage capacity estimation of FSO links with pointing errors over gamma turbulence channels. In Proceedings of the 2016 5th International Conference on Modern Circuits and Systems Technologies (MOCASST), Thessaloniki, Greece, 12–14 May 2016.
37. Jurado-Navas, A.; Garrido-Balsells, J.M.; Paris, J.F.; Puerta-Notario, A. A unifying statistical model for atmospheric optical scintillation. *Numer. Simul. Phys. Eng. Process.* **2011**, *181*, 181–205.
38. Barrios, R.; Dios, F. Exponentiated Weibull distribution family under aperture averaging for Gaussian beam waves. *Opt. Express* **2012**, *20*, 13055–13064. [[CrossRef](#)]
39. Sandalidis, H.G.; Chatzidiamantis, N.D.; Karagiannidis, G.K. A tractable model for turbulence-and misalignment-induced fading in optical wireless systems. *IEEE Commun. Lett.* **2016**, *20*, 1904–1907. [[CrossRef](#)]
40. Nistazakis, H.E.; Tsigopoulos, A.D.; Haniyas, M.P.; Psychogios, C.; Marinou, D.; Aidinis, C.; Tombras, G.S. Estimation of Outage Capacity for Free Space Optical Links over IK and K Turbulent Channels. *Radioengineering* **2011**, *20*, 493–498.
41. Nistazakis, H.E.; Assimakopoulos, V.D.; Tombras, G.S. Performance estimation of free space optical links over negative exponential atmospheric turbulence channels. *OPTIK-Int. J. Light Electron Opt.* **2011**, *122*, 2191–2194. [[CrossRef](#)]

42. Chatzidiamentis, N.D.; Sandalidis, H.G.; Karagiannidis, G.K.; Matthaiou, M. Inverse Gaussian modeling of turbulence-induced fading in free-space optical systems. *J. Light. Technol.* **2011**, *29*, 1590–1596. [[CrossRef](#)]
43. Kedar, D.; Arnon, S. Urban optical wireless communication networks: The main challenges and possible solutions. *IEEE Commun. Mag.* **2004**, *42*, S2–S7. [[CrossRef](#)]
44. Farid, A.A.; Hranilovic, S. Outage capacity optimization for free space optical links with pointing errors. *IEEE/OSA J. Light. Technol.* **2007**, *25*, 1702–1710. [[CrossRef](#)]
45. Sandalidis, H.G.; Tsiftsis, T.A.; Karagiannidis, G.K.; Uysal, M. BER performance of FSO links over strong atmospheric turbulence channels with pointing errors. *IEEE Commun. Lett.* **2008**, *12*, 44–46. [[CrossRef](#)]
46. Al Quwaiee, H.; Yang, H.C.; Alouini, M.S. On the asymptotic capacity of dual-aperture FSO systems with generalized pointing error model. *IEEE Trans. Wirel. Commun.* **2016**, *15*, 6502–6512. [[CrossRef](#)]
47. Boluda-Ruiz, R.; García-Zambrana, A.; Castillo-Vázquez, C.; Castillo-Vázquez, B. Novel approximation of misalignment fading modeled by Beckmann distribution on free-space optical links. *Opt. Express* **2016**, *24*, 22635–22649. [[CrossRef](#)]
48. Jurado-Navas, A.; Garrido-Balsells, J.M.; Paris, J.F.; Castillo-Vázquez, M.; Puerta-Notario, A. Impact of pointing errors on the performance of generalized atmospheric optical channels. *Opt. Express* **2012**, *20*, 12550–12562. [[CrossRef](#)]
49. Varotsos, G.K.; Nistazakis, H.E.; Volos, C.K.; Tombras, G.S. FSO links with diversity pointing errors and temporal broadening of the pulses over weak to strong atmospheric turbulence channels. *Optik* **2016**, *127*, 3402–3409. [[CrossRef](#)]
50. Djordjevic, G.T.; Petkovic, M.I.; Spasic, M.; Antic, D.S. Outage capacity of FSO link with pointing errors and link blockage. *Opt. Express* **2016**, *24*, 219–230. [[CrossRef](#)]
51. Elganimi, T.Y. Performance comparison between OOK, PPM and pam modulation schemes for free space optical (FSO) communication systems: Analytical study. *Int. J. Comput. Appl.* **2013**, *79*, 22–27.
52. Muhammad, S.S.; Javornik, T.; Jelovčan, I.; Ghassemlooy, Z.; Leitgeb, E. Comparison of hard-decision and soft-decision channel coded M-ary PPM performance over free space optical links. *Eur. Trans. Telecommun.* **2009**, *20*, 746–757. [[CrossRef](#)]
53. Gappmair, W.; Hranilovic, S.; Leitgeb, E. Performance of PPM on terrestrial FSO links with turbulence and pointing errors. *IEEE Commun. Lett.* **2010**, *14*, 468–470. [[CrossRef](#)]
54. Song, X.; Yang, F.; Cheng, J.; Al-Dhahir, N.; Xu, Z. Subcarrier phase-shift keying systems with phase errors in lognormal turbulence channels. *J. Light. Technol.* **2015**, *33*, 1896–1904. [[CrossRef](#)]
55. Varotsos, G.K.; Nistazakis, H.E.; Gappmair, W.; Sandalidis, H.G.; Tombras, G.S. SIMO subcarrier PSK FSO links with phase noise and non-zero boresight pointing errors over turbulence channels. *IET Commun.* **2019**, *13*, 831–836. [[CrossRef](#)]
56. Navidpour, S.M.; Uysal, M.; Kavehrad, M. BER performance of free-space optical transmission with spatial diversity. *IEEE Trans. Wirel. Commun.* **2007**, *6*, 2813–2819. [[CrossRef](#)]
57. Tsiftsis, T.A.; Sandalidis, H.G.; Karagiannidis, G.K.; Uysal, M. Optical wireless links with spatial diversity over strong atmospheric turbulence channels. *IEEE Trans. Wirel. Commun.* **2009**, *8*, 951–957. [[CrossRef](#)]
58. Nistazakis, H.E.; Tombras, G.S. On the use of wavelength and time diversity in optical wireless communication systems over gamma–gamma turbulence channels. *Opt. Laser Technol.* **2012**, *44*, 2088–2094. [[CrossRef](#)]
59. Nistazakis, H.E. A time-diversity scheme for wireless optical links over exponentially modeled turbulence channels. *Opt.-Int. J. Light Electron Opt.* **2013**, *124*, 1386–1391. [[CrossRef](#)]
60. Shah, D.; Kothari, D.; Ghosh, A. Performance of free-space optical link with wavelength diversity over exponentiated Weibull channel. *Opt. Eng.* **2016**, *55*, 999–1002. [[CrossRef](#)]
61. Prabu, K.; Cheepalli, S.; Kumar, D.S. Analysis of PolSK based FSO system using wavelength and time diversity over strong atmospheric turbulence with pointing errors. *Opt. Commun.* **2014**, *324*, 318–323. [[CrossRef](#)]
62. Prabu, K.; Kumar, D.S. BER analysis of DPSK–SIM over MIMO free space optical links with misalignment. *Opt. Int. J. Light Electron Opt.* **2014**, *125*, 5176–5180. [[CrossRef](#)]
63. Garcia-Zambrana, A.; Boluda-Ruiz, R.; Castillo-Vazquez, C.; Castillo-Vazquez, B. Transmit alternate laser selection with time diversity for FSO communications. *Opt. Express* **2014**, *22*, 23861–23874. [[CrossRef](#)]
64. Varotsos, G.K.; Nistazakis, H.E.; Gappmair, W.; Sandalidis, H.G.; Tombras, G.S. DF relayed subcarrier FSO links over Malaga turbulence channels with phase noise and non-zero boresight pointing errors. *Appl. Sci.* **2018**, *8*, 664. [[CrossRef](#)]
65. Varotsos, G.K.; Stassinakis, A.N.; Nistazakis, H.E.; Tsigopoulos, A.D.; Peppas, K.P.; Aidinis, C.J.; Tombras, G.S. Probability of fade estimation for FSO links with time dispersion and turbulence modeled with the gamma–gamma or the IK distribution. *Optik* **2014**, *125*, 7191–7197. [[CrossRef](#)]
66. Lu, H.; Zhao, W.; Xie, X. Analysis of temporal broadening of optical pulses by atmospheric dispersion in laser communication system. *Opt. Commun.* **2012**, *285*, 3169–3173. [[CrossRef](#)]
67. Stassinakis, A.N.; Nistazakis, H.E.; Peppas, K.P.; Tombras, G.S. Improving the availability of terrestrial FSO links over log normal atmospheric turbulence channels using dispersive chirped Gaussian pulses. *Opt. Laser Technol.* **2013**, *54*, 329–334. [[CrossRef](#)]
68. Sova, R.M.; Sluz, J.E.; Young, D.W.; Juarez, J.C.; Dwivedi, A.; Demidovich, N.M., III; Graves, J.E.; Northcott, M.; Douglas, J.; Phillips, J.; et al. 80 Gb/s free-space optical communication demonstration between an aerostat and a ground terminal. In *Free-Space Laser Communications VI*; SPIE: Bellingham, WA, USA, 2006; Volume 6304, pp. 267–276.
69. Ciaramella, E.; Arimoto, Y.; Contestabile, G.; Presi, M.; D’Errico, A.; Guarino, V.; Matsumoto, M. 1.28 Terabit/s (32 × 40 Gbit/s) WDM transmission system for free space optical communications. *IEEE J. Sel. Areas Commun.* **2009**, *27*, 1639–1645. [[CrossRef](#)]

70. Awan, M.S.; Csurgai-Horváth, L.; Muhammad, S.S.; Leitgeb, E.; Nadeem, F.; Khan, M.S. Characterization of Fog and Snow Attenuations for Free-Space Optical Propagation. *J. Commun.* **2009**, *4*, 533–545. [[CrossRef](#)]
71. Esmail, M.A.; Ragheb, A.; Fathallah, H.; Alouini, M.S. Experimental demonstration of outdoor 2.2 Tbps super-channel FSO transmission system. In Proceedings of the 2016 IEEE International Conference on Communications Workshops (ICC), Kuala Lumpur, Malaysia, 23–27 May 2016.
72. Alheadary, W.G.; Park, K.H.; Alfaraj, N.; Guo, Y.; Stegenburgs, E.; Ng, T.K.; Ooi, B.S.; Alouini, M.S. Free-space optical channel characterization and experimental validation in a coastal environment. *Opt. Express* **2018**, *26*, 6614–6628. [[CrossRef](#)]
73. Lionis, A.; Peppas, K.; Nistazakis, H.E.; Tsigopoulos, A.; Cohn, K. Statistical modeling of received signal strength for an FSO link over maritime environment. *Opt. Commun.* **2021**, *489*, 126858. [[CrossRef](#)]
74. Arya, S.; Chung, Y.H. Amplify-and-forward multihop non-line-of-sight ultraviolet communication in the gamma–gamma fading channel. *J. Opt. Commun. Netw.* **2019**, *11*, 422–436. [[CrossRef](#)]
75. Xu, Z.; Sadler, B.M. Ultraviolet communications: Potential and state-of-the-art. *IEEE Commun. Mag.* **2008**, *46*, 67–73.
76. Yuan, R.; Ma, J. Review of ultraviolet non-line-of-sight communication. *China Commun.* **2016**, *13*, 63–75. [[CrossRef](#)]
77. Shaw, G.A.; Siegel, A.M.; Model, J. Extending the range and performance of non-line-of-sight ultraviolet communication links. In *Unattended Ground, Sea, and Air Sensor Technologies and Applications VIII*; SPIE: Orlando, FL, USA, 2006; Volume 6231, pp. 93–104.
78. Xu, Z.; Chen, G.; Abou-Galala, F.; Lonardi, M. Experimental Performance Evaluation of Non-Line-of-Sight Ultraviolet Communication Systems. In *Free Space Laser Communications VII*; SPIE: San Diego, CA, USA, 2007; Volume 6709, pp. 287–298.
79. Shaw, G.A.; Siegel, A.M.; Model, J.; Geboff, A. Deep UV photon counting detectors and applications. In *Advanced Photon Counting Techniques III*; SPIE: Orlando, FL, USA, 2009; Volume 7320, pp. 88–102.
80. Ding, H.; Sadler, B.M.; Chen, G.; Xu, Z. Modeling and characterization of ultraviolet scattering communication channels. In *Advanced Optical Wireless Communication Systems*, 1st ed.; Arnon, S., Barry, J., Karagiannidis, G.K., Schober, R., Uysal, M., Eds.; Cambridge University Press: Cambridge, UK, 2012; pp. 177–200.
81. Chen, G.; Xu, Z.; Ding, H.; Sadler, B.M. Path loss modeling and performance trade-off study for short-range non-line-of-sight ultraviolet communications. *Opt. Express* **2009**, *17*, 3929–3940. [[CrossRef](#)]
82. He, Q.; Sadler, B.M.; Xu, Z. Modulation and coding tradeoffs for non-line-of-sight ultraviolet communications. In *Free-Space Laser Communications IX*; SPIE: San Diego, CA, USA, 2009; Volume 7464, pp. 151–162.
83. He, Q.; Sadler, B.M.; Xu, Z. On the achievable performance of non-line-of-sight ultraviolet communications. In *Applications of Lasers for Sensing and Free Space Communications*; Optica Publishing Group: San Diego, CA, USA, 2010; p. LSMB2.
84. He, Q.; Xu, Z.; Sadler, B.M. Performance of short-range non-line-of-sight LED-based ultraviolet communication receivers. *Opt. Express* **2010**, *18*, 12226–12238. [[CrossRef](#)]
85. Wang, L.; Li, Y.; Xu, Z.; Sadler, B.M. Wireless ultraviolet network models and performance in noncoplanar geometry. In Proceedings of the 2010 IEEE Globecom Workshops, Miami, FL, USA, 6–10 December 2010.
86. Wang, P.; Xu, Z. Characteristics of ultraviolet scattering and turbulent channels. *Opt. Lett.* **2013**, *38*, 2773–2775. [[CrossRef](#)]
87. Kedar, D.; Arnon, S. Evaluation of coherence interference in optical wireless communication through multi-scattering channels. *Appl. Opt.* **2006**, *45*, 3263–3269. [[CrossRef](#)]
88. Kedar, S.; Arnon, S. Non-line-of-sight optical wireless sensor network operating in multi scattering channel. *Appl. Opt.* **2006**, *45*, 8454–8461. [[CrossRef](#)]
89. Gupta, A.; Brandt-Pearce, M. Receiver design for shot noise limited MIMO FSO/UV communication systems. In Proceedings of the IEEE Globecom Workshop on Optical Wireless Communications, Anaheim, CA, USA, 3–7 December 2012.
90. Noshad, M.; Brandt-Pearce, M.; Wilson, S.G. NLOS UV communications using M-ary spectral amplitude coding. *IEEE Trans. Commun.* **2013**, *61*, 1544–1553. [[CrossRef](#)]
91. Xiao, H.; Zuo, Y.; Wu, J.; Li, Y.; Lin, J. Bit-error-rate performance of non-line-of-sight UV transmission with spatial diversity reception. *Opt. Lett.* **2012**, *37*, 4143–4145. [[CrossRef](#)]
92. Hutt, D.L.; Tofsted, D.H. Effect of atmospheric turbulence on propagation of ultraviolet radiation. *Opt. Laser Technol.* **2000**, *32*, 39–48. [[CrossRef](#)]
93. Ding, H.; Chen, G.; Majumdar, A.K.; Sadler, B.M.; Xu, Z. Turbulence modeling for non-line-of-sight ultraviolet scattering channels. In *Atmospheric Propagation VIII*; SPIE: Orlando, FL, USA, 2011; Volume 8038, pp. 195–202.
94. Zuo, Y.; Xiao, H.; Wu, J.; Hong, X.; Lin, J. Effect of atmospheric turbulence on non-line-of-sight ultraviolet communications. In Proceedings of the 2012 IEEE 23rd International Symposium on Personal, Indoor and Mobile Radio Communications—(PIMRC), Sydney, NSW, Australia, 9–12 September 2012.
95. Xiao, H.; Zuo, Y.; Fan, C.; Wu, C.; Wu, J. Non-line-of-sight ultraviolet channel parameters estimation in turbulence atmosphere. In Proceedings of the 2012 Asia Communications and Photonics Conference (ACP), Guangzhou, China, 7–10 November 2012.
96. Liu, W.; Xu, Z. Characteristics of optical scattering and turbulence communication channels. In Proceedings of the 2014 48th Asilomar Conference on Signals, Systems and Computers, Pacific Grove, CA, USA, 2–5 November 2014.
97. Liao, L.; Li, Z.; Lang, T.; Sadler, B.M.; Chen, G. Turbulence channel test and analysis for NLOS UV communication. In *Laser Communication and Propagation through the Atmosphere and Oceans III*; SPIE: San Diego, CA, USA, 2014; Volume 9224, pp. 411–416.
98. Liao, L.; Li, Z.; Lang, T.; Chen, G. UV LED array based NLOS UV turbulence channel modeling and experimental verification. *Opt. Express* **2015**, *23*, 21825–21835. [[CrossRef](#)]

99. Li, B.; Wang, H.; Wu, X.; Song, B.; Hu, H. Modification of atmospheric extinction coefficient of non-line-of-sight ultraviolet communication under weak turbulence. *Opt. Laser Technol.* **2015**, *66*, 45–51. [[CrossRef](#)]
100. Wang, K.; Gong, C.; Zou, D.; Xu, Z. Turbulence channel modeling and non-parametric estimation for optical wireless scattering communication. *J. Light. Technol.* **2017**, *35*, 2746–2756. [[CrossRef](#)]
101. Chen, G.; Liao, L.; Li, Z.; Drost, R.J.; Sadler, M.B. Experimental and simulated evaluation of long distance NLOS UV communication. In Proceedings of the 9th International Symposium on Communication Systems, Networks Digital Signal Processing (CSNDSP), Manchester, UK, 23–25 July 2014.
102. Raptis, N.; Pikasis, E.; Syvridis, D. Performance evaluation of modulation and multiple access schemes in ultraviolet optical wireless connections for two atmosphere thickness cases. *JOSA A* **2016**, *33*, 1628–1640. [[CrossRef](#)]
103. Arya, S.; Chung, Y.H. A unified statistical model for Málaga distributed optical scattering communications. *Opt. Commun.* **2020**, *463*, 125402. [[CrossRef](#)]
104. Arya, S.; Chung, Y.H. Non-line-of-sight ultraviolet communication with receiver diversity in atmospheric turbulence. *IEEE Photonics Technol. Lett.* **2018**, *30*, 895–898. [[CrossRef](#)]
105. Arya, S.; Chung, Y.H. Maximal Selective Transmit Diversity for Petahertz Wireless Communications With Continuous Waveform Detector. *IEEE Access* **2021**, *9*, 118005–118018. [[CrossRef](#)]
106. Varotsos, G.K.; Nistazakis, H.E.; Kapotis, E.; Chatzikontis, E.V.; Aidinis, K.; Volos, C.K. ABER Estimation of NLOS UV Links with Time Diversity over K-Turbulent Channels and Path Loss. In Proceedings of the 2023 12th International Conference on Modern Circuits and Systems Technologies (MOCAST), Athens, Greece, 28–30 June 2023.
107. Gong, C.; Xu, Z. Linear receivers for optical wireless scattering communication with multiple photon detectors. In Proceedings of the 2014 IEEE Globecom Workshops (GC Wkshps), Austin, TX, USA, 8–12 December 2014.
108. Huang, B.; Gong, C.; Xu, Z. Correlation study for single-input multiple-output optical wireless scattering channels. In Proceedings of the 2014 48th Asilomar Conference on Signals, Systems and Computers, Pacific Grove, CA, USA, 2–5 November 2014.
109. Guo, L.; Liu, K.; Meng, D.; Mu, X.; Han, D. Simulation and experimental research on the Alamouti code for ultraviolet communication. *Opt. Eng.* **2016**, *55*, 015101. [[CrossRef](#)]
110. Meng, X.; Zhang, M.; Han, D.; Song, L.; Luo, P. Experimental study on 1×4 real-time SIMO diversity reception scheme for a ultraviolet communication system. In Proceedings of the 2015 20th European Conference on Networks and Optical Communications-(NOC), London, UK, 30 June–2 July 2015.
111. Cong, R.; Zuo, Y.; Li, F.; Meng, L.; Qin, H.; Zhang, J.; Wu, J. Experimental performance of 2×2 Alamouti space-time coding non-line-of-sight ultraviolet communication system. In Proceedings of the Asia Communications and Photonics Conference, Guangzhou, China, 10–13 November 2017.
112. Ardakani, M.H.; Heidarpour, A.R.; Uysal, M. Performance analysis of MIMO NLOS UV communications over atmospheric turbulence channels. In Proceedings of the Workshop on Optical Wireless Communications (OWC 2016), Doha, Qatar, 3 April 2016.
113. Han, D.; Zhang, M.; Li, Q. Experimental measurement of link gain and correlation in a single-input multiple-output ultraviolet communication system with diversity reception. *Opt. Eng.* **2017**, *56*, 084108. [[CrossRef](#)]
114. Zou, D.; Gong, C.; Xu, Z. Secrecy rate of MISO optical wireless scattering communications. *IEEE Trans. Commun.* **2017**, *66*, 225–238. [[CrossRef](#)]
115. Mou, W.; Pu, T.; Yang, W.; Zheng, J.; Tang, X. Secrecy performance of noncoplanar SIMOME NLOS ultraviolet communications over turbulence channels. *Opt. Commun.* **2019**, *433*, 262–267. [[CrossRef](#)]
116. Qin, H.; Zuo, Y.; Li, F.; Cong, R.; Meng, L.; Wu, J. Noncoplanar geometry for mobile NLOS MIMO ultraviolet communication with linear complexity signal detection. *IEEE Photonics J.* **2017**, *9*, 1–12. [[CrossRef](#)]
117. Gu, Y.; Zhang, M.; Han, D.; Chen, Q.; Ghassemlooy, Z. Experimental research on SOPP-OSTBC scheme in UV communication with concise 2-PPM. In Proceedings of the 2017 Conference on Lasers and Electro-Optics Pacific Rim (CLEO-PR), Singapore, 31 July–4 August 2017.
118. Alkhazragi, O.; Hu, F.; Zou, P.; Ha, Y.; Kang, C.H.; Mao, Y.; Ng, T.K.; Chi, N.; Ooi, B.S. Gbit/s ultraviolet-C diffuse-line-of-sight communication based on probabilistically shaped DMT and diversity reception. *Opt. Express* **2020**, *28*, 9111–9122. [[CrossRef](#)] [[PubMed](#)]
119. Bhatia, V.; Jain, S.; Garg, K.; Mitra, R. Performance analysis of RKHS based detectors for nonlinear NLOS ultraviolet communications. *IEEE Trans. Veh. Technol.* **2021**, *70*, 3625–3639. [[CrossRef](#)]
120. Han, D.; Liu, Y.; Zhang, K.; Luo, P.; Zhang, M. Theoretical and experimental research on diversity reception technology in NLOS UV communication system. *Opt. Express* **2012**, *20*, 15833–15842. [[CrossRef](#)]
121. Geller, M.; Keenan, T.E.; Altman, D.E.; Patterson, R.H. *Optical Non-Line-of-Sight Covert, Secure High Data Communication System*; Patent Department of the Navy: San Diego, CA, USA, 1985.
122. Puschell, J.J.; Bayse, R. High data rate ultraviolet communication systems for the tactical battlefield. In Proceedings of the Conference Proceedings on Tactical Communications, Fort Wayne, IN, USA, 24–26 April 1990.
123. Sun, X.; Zhang, Z.; Chaaban, A.; Ng, T.K.; Shen, C.; Chen, R.; Yan, J.; Sun, H.; Li, X.; Wang, J.; et al. 71-Mbit/s ultraviolet-B LED communication link based on 8-QAM-OFDM modulation. *Opt. Express* **2017**, *25*, 23267–23274. [[CrossRef](#)]
124. He, X.; Xie, E.; Islim, M.S.; Purwita, A.A.; McKendry, J.J.; Gu, E.; Haas, H.; Dawson, M.D. 1 Gbps free-space deep-ultraviolet communications based on III-nitride micro-LEDs emitting at 262 nm. *Photonics Res.* **2019**, *7*, B41–B47. [[CrossRef](#)]

125. He, Q.; Xu, Z.; Brian, M.S. Non-line-of-sight serial relayed link for optical wireless communications. In Proceedings of the 2010-Milcom 2010 Military Communications Conference, San Jose, CA, USA, 31 October–3 November 2010.
126. Ardakani, M.H.; Heidarpour, A.R.; Uysal, M. Performance analysis of relay-assisted NLOS ultraviolet communications over turbulence channels. *J. Opt. Commun. Netw.* **2017**, *9*, 109–118. [[CrossRef](#)]
127. Ardakani, M.H.; Uysal, M. Relay-assisted OFDM for ultraviolet communications: Performance analysis and optimization. *IEEE Trans. Wirel. Commun.* **2016**, *16*, 607–618. [[CrossRef](#)]
128. Varotsos, G.K.; Nistazakis, H.E.; Aidinis, K.; Jaber, F.; Rahman, K.K.M. Signal intensity estimation in transdermal optical wireless links with stochastic pointing error effect. *Technologies* **2020**, *8*, 60. [[CrossRef](#)]
129. Liu, T.; Bihr, U.; Anis, S.M.; Ortmanns, M. Optical transcutaneous link for low power, high data rate telemetry. In Proceedings of the 2012 Annual International Conference of the IEEE Engineering in Medicine and Biology Society (EMBC), San Diego, CA, USA, 28 August–1 September 2012.
130. Gil, Y.; Rotter, N.; Arnon, S. Feasibility of retroreflective transdermal optical wireless communication. *Appl. Opt.* **2012**, *51*, 4232–4239. [[CrossRef](#)] [[PubMed](#)]
131. Abita, J.L.; Schneider, W. Transdermal Optical Communications. *John Hopkins APL Tech. Dig.* **2004**, *25*, 261–268.
132. Liu, T.; Bihr, U.; Becker, J.; Anders, J.; Ortmanns, M. In vivo verification of a 100 Mbps transcutaneous optical telemetric link. In Proceedings of the Biomedical Circuits and Systems Conference (BioCAS), Lausanne, Switzerland, 22–24 October 2014.
133. Ackermann, D.M.; Smith, B.; Wang, X.F.; Kilgore, K.L.; Peckham, P.H. Designing the optical interface of a transcutaneous optical telemetry link. *IEEE Trans. Biomed. Eng.* **2008**, *55*, 1365–1373. [[CrossRef](#)] [[PubMed](#)]
134. Parmentier, S.; Fontaine, R.; Roy, Y. Laser diode used in 16 Mb/s, 10 mW optical transcutaneous telemetry system. In Proceedings of the 2008 IEEE Biomedical Circuits and Systems Conference, Baltimore, MD, USA, 20–22 November 2008.
135. Miranda, H.; Gilja, V.; Chestek, C.A.; Shenoy, K.V.; Meng, T.H.; Hermes, D. A high-rate long-range wireless transmission system for simultaneous multichannel neural recording applications. *IEEE Trans. Biomed. Circuits Syst.* **2010**, *4*, 181–191. [[CrossRef](#)]
136. Liu, T.; Anders, J.; Ortmanns, M. Bidirectional optical transcutaneous telemetric link for brain machine interface. *Electron. Lett.* **2015**, *51*, 1969–1971. [[CrossRef](#)]
137. Trevlakis, S.E.; Boulogeorgos, A.A.A.; Sofotasios, P.C.; Muhaidat, S.; Karagiannidis, G.K. Optical wireless cochlear implants. *Biomed. Opt. Express* **2019**, *10*, 707–730. [[CrossRef](#)]
138. Trevlakis, S.E.; Boulogeorgos, A.A.A.; Chatzidiamantis, N.D.; Karagiannidis, G.K. All-optical cochlear implants. *IEEE Trans. Mol. Biol. Multi-Scale Commun.* **2020**, *6*, 13–24. [[CrossRef](#)]
139. Trevlakis, S.E.; Boulogeorgos, A.A.A.; Karagiannidis, G.K. On the impact of misalignment fading in transdermal optical wireless communications. In Proceedings of the 7th International Conference on Modern Circuits and Systems Technologies (MOCAST), Thessaloniki, Greece, 7–9 May 2018.
140. Trevlakis, S.E.; Boulogeorgos, A.A.A.; Karagiannidis, G. Signal quality assessment for transdermal optical wireless communications under pointing errors. *Technologies* **2018**, *6*, 109. [[CrossRef](#)]
141. Trevlakis, S.E.; Boulogeorgos, A.A.A.; Karagiannidis, G.K. Outage performance of transdermal optical wireless links in the presence of pointing errors. In Proceedings of the 2018 IEEE 19th International Workshop on Signal Processing Advances in Wireless Communications (SPAWC), Kalamata, Greece, 25–28 June 2018.
142. Boulogeorgos, A.A.A.; Trevlakis, S.E.; Chatzidiamantis, N.D. Optical wireless communications for in-body and transdermal biomedical applications. *IEEE Commun. Mag.* **2021**, *59*, 119–125. [[CrossRef](#)]
143. Varotsos, G.K.; Nistazakis, H.E.; Tombras, G.S.; Aidinis, K.; Jaber, F.; Rahman, M. On the use of diversity in transdermal optical wireless links with nonzero boresight pointing errors for outage performance estimation. In Proceedings of the 2019 8th International Conference on Modern Circuits and Systems Technologies (MOCAST), Thessaloniki, Greece, 13–15 May 2019.
144. Varotsos, G.K.; Nistazakis, H.E.; Aidinis, K.; Roumelas, G.D.; Jaber, F.; Rahman, K.K.M. Modulated retro-reflector transdermal optical wireless communication systems with wavelength diversity over skin-induced attenuation and pointing errors. In Proceedings of the 2020 IEEE International Symposium on Signal Processing and Information Technology (ISSPIT), Ajman, United Arab Emirates, 10–12 December 2019.
145. Varotsos, G.K.; Nistazakis, H.E.; Aidinis, K.; Jaber, F.; Nasor, M.; Rahman, K.K.M. Error performance estimation of modulated retroreflective transdermal optical wireless links with diversity under generalized pointing errors. *Telecom* **2021**, *2*, 167–180. [[CrossRef](#)]
146. Diamantoulakis, P.D.; Karagiannidis, G.K.; Ding, Z. Simultaneous lightwave information and power transfer (SLIPT). *IEEE Trans. Green Commun. Netw.* **2018**, *2*, 764–773. [[CrossRef](#)]
147. Pan, G.; Diamantoulakis, P.D.; Ma, Z.; Ding, Z.; Karagiannidis, G.K. Simultaneous lightwave information and power transfer: Policies, techniques, and future directions. *IEEE Access* **2019**, *7*, 28250–28257. [[CrossRef](#)]
148. Guillory, K.S.; Misener, A.K.; Pungor, A. Hybrid RF/IR transcutaneous telemetry for power and high-bandwidth data. In Proceedings of the 26th Annual International Conference of the IEEE Engineering in Medicine and Biology Society, San Francisco, CA, USA, 1–4 September 2005.
149. Zeng, F.G.; Rebscher, S.; Harrison, W.; Sun, X.; Feng, H. Cochlear implants: System design, integration, and evaluation. *IEEE Rev. Biomed. Eng.* **2008**, *1*, 115–142. [[CrossRef](#)] [[PubMed](#)]

150. Liu, T.; Bihl, U.; Anders, J.; Ortmanns, M. Performance evaluation of a low power optical wireless link for biomedical data transfer. In Proceedings of the 2014 IEEE International Symposium on Circuits and Systems (ISCAS), Melbourne, Australia, 1–5 June 2014.
151. Lange, S.; Xu, H.; Lang, C.; Pless, H.; Becker, J.; Tiedtke, H.J.; Hennig, E.; Ortmanns, M. An AC-powered optical receiver consuming 270 μ W for transcutaneous 2Mb/s data transfer. In Proceedings of the 2011 IEEE International Solid-State Circuits Conference, San Francisco, CA, USA, 20–24 February 2011.

Disclaimer/Publisher’s Note: The statements, opinions and data contained in all publications are solely those of the individual author(s) and contributor(s) and not of MDPI and/or the editor(s). MDPI and/or the editor(s) disclaim responsibility for any injury to people or property resulting from any ideas, methods, instructions or products referred to in the content.